Available online at www.sciencedirect.com
SCIENCE DIRECT®
Geochimica et Cosmochimica Acta 70 (2006) 3778–3802
Geochimica
www.elsevier.com/locate/gca

A predictive model (ETLM) for As(III) adsorption and surface speciation on oxides consistent with spectroscopic data

Dimitri A. Sverjensky *, Keisuke Fukushi

Department of Earth and Planetary Sciences, The Johns Hopkins University, Baltimore, MD 21218, USA

Received 21 November 2005; accepted in revised form 18 May 2006

Abstract

Arsenic(III) adsorption reactions are thought to play a critical role in the mobility of arsenic in the environment. It is the nature of the As(III) surface species that must be known on a wide variety of minerals and over a range of pH, ionic strength and surface coverage in order to be able to predict adsorption behavior. EXAFS and XANES spectroscopic studies have identified bidentate, binuclear inner-sphere surface species and/or an outer-sphere species, but only a few oxides have been examined. These results need to be integrated with a predictive surface complexation model in order to ascertain the environmental conditions under which the different surface species may be important on a wide range of solids. In the present study, the surface species information from XAFS and XANES studies has been built into a recent extension of the triple-layer model (ETLM) for the formation of inner-sphere complexes of anions that takes into account the electrostatics of water dipole desorption during ligand exchange reactions. The ETLM has been applied to regress surface titration, proton coadsorption, and As(III) adsorption data over extensive ranges of pH, ionic strength, electrolyte type and surface coverage for magnetite, goethite, gibbsite, amorphous hydrous alumina, hydrous ferric oxide (HFO), ferrihydrite, and amorphous iron oxide. Two principal reactions forming inner- and outer-sphere As(III) surface species,

$$2\,{>}\mathrm{SOH} + \mathrm{As(OH)_3^0} = (>\mathrm{SO})_2\mathrm{As(OH)^0} + 2\mathrm{H_2O}$$

and

$$>\mathrm{SOH} + \mathrm{As(OH)_3^0} => \mathrm{SOH_2^+\_AsO(OH)_2^-},$$

respectively, were found to be consistent with most of the data. The proportions of these species vary systematically. Under some circumstances, on ferrihydrite, am.FeO, and HFO an additional inner-sphere deprotonated, bidentate, binuclear species and an additional outer-sphere species represented by

$$2\,{>}\mathrm{SOH} + \mathrm{As(OH)_3^0} = (>\mathrm{SO})_2\mathrm{AsO^-} + \mathrm{H^+} + 2\mathrm{H_2O}$$

and

$$2\,{>}\mathrm{SOH} + \mathrm{H^+} + \mathrm{As(OH)_3^0} = (>\mathrm{SOH_2^+})_2\mathrm{\_AsO(OH)_2^-},$$

respectively, were needed. Expressing the equilibrium constants with respect to internally consistent site-occupancy standard states for As(III) adsorption on different solids permits systematic differences to be examined and explained with Born solvation theory. As a result, a set of predictive equations for As(III) adsorption equilibrium constants on all oxides, including both amorphous and poorly crystalline oxides, enables prediction of the surface speciation of As(III) over wide ranges of pH, ionic strength, electrolyte type and surface coverage.

* Corresponding author. Fax: +1 410 516 7933.
E-mail addresses: sver@jhu.edu (D.A. Sverjensky), fukushi@jhu.edu (K. Fukushi).

0016-7037/$ - see front matter © 2006 Elsevier Inc. All rights reserved.
doi:10.1016/j.gca.2006.05.012

1. Introduction

An understanding of the geochemistry of arsenic in low-temperature sedimentary environments has become critical to the development of safe drinking water and food supplies in many countries (Smedley and Kinniburgh, 2002; Williams et al., 2005). Of the processes influencing arsenic mobility, arsenic adsorption reactions to oxide mineral surfaces are thought to strongly influence the concentrations of dissolved arsenic in the environment (Nickson et al., 2000, 2005). Under the reducing conditions typical of many groundwaters, arsenic adsorption is dominated by As(III) species which can adsorb strongly depending on the type of oxide and the presence of other anions (Wilkie and Hering, 1996; Dixit and Hering, 2003). It is the nature of the adsorbed As(III) species that must be known on a wide variety of minerals and over a range of pH, ionic strength and surface coverage in order to be able to predict the adsorption behavior and therefore the mobility of As(III) in the environment.

The surface speciation of adsorbed As(III) on oxides has been studied experimentally through X-ray and infrared spectroscopic studies. An inner-sphere, bidentate–binuclear species has been established by EXAFS for As(III) adsorbed on goethite from 0.001 M NaCl solutions over the pH range 6.4–8.6 and surface coverages from 1.9 to 4.4 μmol m^{-2} (Manning et al., 1998). The same type of inner-sphere complex was detected on both goethite and lepidocrocite (Farquhar et al., 2002). On β-$Al(OH)_3$ (bayerite), an inner-sphere, bidentate–binuclear species plus an outer-sphere complex have been established by EXAFS and XANES for As(III) adsorbed from 0.01 to 0.8 M $NaNO_3$ solutions at pH values of 5.5 and 8.0 and a surface coverage of 1.6 μmol m^{-2} (Arai et al., 2001). In addition, the latter study established that the proportion of outer- to inner-sphere complexes increased with pH and decreased with ionic strength. The state of protonation of the arsenic surface species cannot be established by X-ray studies.

In contrast to X-ray studies, Fourier transform infrared (FTIR) spectroscopic studies do have the potential for providing information about both the structure and state of protonation of adsorbed arsenic (Suarez et al., 1998). An FTIR study of As(III) on dry goethite has reported a bidentate–binuclear complex (Sun and Doner, 1996), but results on dry samples may differ significantly from those under in situ conditions (Hug, 1997; Paul et al., 2005). Based on a combination of infrared spectroscopic, sorption and electrophoretic mobility measurements, it has been concluded that As(III) forms inner- and outer-sphere complexes on amorphous iron hydroxide and outer-sphere complexes on amorphous aluminum hydroxide (Goldberg and Johnston, 2001). To summarize the X-ray and infrared spectroscopic results, both inner- and outer-sphere surface complexes have been detected, but it remains to be established under what ranges of conditions these species might be present on a variety of oxides. Where the inner-sphere complex has been detected, it has a bidentate, binuclear structure. Definitive experimental evidence of the state of protonation of the two surface As(III) species is still lacking. It should also perhaps be emphasized that distinguishing between a true outer-sphere complex (with waters of solvation associated with the arsenite) and a hydrogen-bonded complex may be difficult experimentally.

The surface speciation and state of protonation of adsorbed As(III) have also been addressed through theoretical DFT and MO/DFT calculations. Using gas-phase DFT calculations, the most stable surface As(III) species was found to be a bidentate–binuclear species $(>FeO)_2As(OH)^0$ (Zhang et al., 2005). Using MO/DFT calculations (Kubicki, 2005), inner-sphere bidentate binuclear binding of As(III) was compared on model Fe-clusters versus model Al-clusters under conditions designed to approximate positively charged and neutral surfaces. The results indicate a strong preference for As(III) to bind to Fe- relative to Al-surfaces, as well as a strong preference for binding on the neutral surfaces relative to positively charged surfaces.

Inferences about the surface speciation and state of protonation of adsorbed As(III) have been made based on experimental studies of proton surface titration in the presence of arsenic and proton co-adsorption with arsenic (Jain et al., 1999a). At high arsenic coverages these experiments probably reflect surface processes other than just adsorption (Jain et al., 1999b; Stanforth, 1999), but at the lowest surface coverages they provide valuable constraints on the state of protonation of surface arsenic species. A combination of mono- and bidentate surface species with protonation at low pH has been inferred from trends of the data with pH and surface loading (Jain et al., 1999a). However, it is impossible to infer specific reaction stoichiometries because the experimental data represent net protonation changes in response to changes in pH and arsenic levels which result from redistribution of all surface species, not just As-bearing species. Consequently, such experimental data are best used as constraints on surface complexation models which account for a variety of surface reactions simultaneously.

Surface complexation models that describe the bulk adsorption of As(III) have the capability to define the state of protonation of the As(III) surface species, particularly when integrated with spectroscopic and electrophoretic mobility studies (Manning and Goldberg, 1997; Manning et al., 1998; Goldberg and Johnston, 2001). However, the structures of the surface species used to date (Dixit and Hering, 2003; Weerasooriya et al., 2003) have not always been consistent with the XAS studies summarized above. Nor has there yet been an attempt to account quantitatively for the proton surface charge, proton coadsorption, and electrokinetic data. An additional limitation of previous surface complexation models of As(III) adsorption is that the models are only usable over limited ranges of ionic strength, surface coverage or type of electrolyte or oxide. For example, As(III) adsorption has been modeled using the Constant Capacitance Model (CCM) when the ionic strength dependence of the adsorption is small, but switch-

ing to the triple-layer model (TLM) when the ionic strength dependence is large (Goldberg and Johnston, 2001). A second example arises from failure to recognize that the hypothetical 1.0 molar standard state for surface species frequently adopted in surface complexation studies includes a dependence on site density and BET surface area (Sverjensky, 2003). For example, when the Diffuse Double Layer Model (DLM) has been used to model As(III) adsorption on three different iron oxides for a single ionic strength and electrolyte (Dixit and Hering, 2003), the magnitudes of the equilibrium constants are not directly comparable without correction for differences in site density and surface area. There is clearly a need for a single model for As(III) adsorption consistent with spectroscopic results and molecular modeling, surface titration, proton coadsorption and electrophoretic mobility data in the presence of As(III), and As(III) adsorption data over wide ranges of pH, ionic strength, electrolyte type and surface coverage for all oxides, and consistent with a set of equilibrium constants referring to a single set of standard states independent of the physical properties of individual samples.

In the present study, we build on the XAFS and XANES studies summarized above to select model inner- and outer-sphere (or H-bonded) As(III) surface species. In the surface complexation calculations we use the term outer-sphere to include true outer-sphere as well as hydrogen-bonded species. The model inner- and outer-sphere species are used as input to an extended triple layer model (ETLM) recently developed to account for the electrostatic effects of water dipole desorption during inner-sphere surface complexation, as well as outer-sphere complexation (Sverjensky and Fukushi, 2006). The basis for application of this model is described below. We investigate the applicability of the spectroscopically identified species, and obtain their states of protonation and relative abundances, by fitting adsorption, proton surface titration and proton coadsorption data for arsenite on magnetite, goethite, gibbsite, amorphous hydrous alumina, hydrous ferric oxide (HFO), ferrihydrite, and amorphous iron oxide (Wilkie and Hering, 1996; Jain et al., 1999a; Jain and Loeppert, 2000; Goldberg and Johnston, 2001; Dixit and Hering, 2003; Weerasooriya et al., 2003). These data were selected to cover wider ranges of pH, ionic strength, surface coverage, and particularly, different types of oxide than have been investigated spectroscopically. Additional data for amorphous iron hydroxide, ferrihydrite and goethite (Pierce and Moore, 1980; Pierce and Moore, 1982; Grafe et al., 2001; Grafe et al., 2002) were not used in the present study, but have already been compared by Dixit and Hering (2003).

The results of the present calculations provide a basis for the understanding and prediction of arsenite surface speciation on all oxides. Furthermore, by adopting an internally consistent set of standard states, systematic differences in the equilibrium constants for the surface As(III) species from one oxide to another can be established and explained with the aid of Born solvation theory. In turn, this makes it possible to predict arsenite adsorption and surface speciation on all oxides in simple electrolyte systems. The results of the present study represent a first step towards addressing more complex systems relevant to natural waters.

2. Integration of spectroscopic results with surface complexation modeling

2.1. Approaches

Integration of experimental spectroscopic results for anion surface speciation with surface complexation models referring to a wide range of pH, ionic strength, surface coverage and type of oxide has become a major challenge (Suarez et al., 1998; Hiemstra and van Riemsdijk, 1999; Blesa et al., 2000; Goldberg and Johnston, 2001). In the Charge Distribution (CD) approach for anion adsorption (Hiemstra and van Riemsdijk, 1999; Villalobos and Leckie, 2001; Arai et al., 2004), spectroscopic results are used to guide the choice of the structure of the surface species and the charge of the adsorbing anion is envisioned as being split between two adsorption planes according to a splitting factor (f). In addition to the equilibrium constant for adsorption, f often becomes a fit parameter (Hiemstra and van Riemsdijk, 1996; Filius et al., 1997; Geelhoed et al., 1997; Rietra et al., 1999; Hiemstra and van Riemsdijk, 2000; Rietra et al., 2001a,b). Model predictions of adsorption as a function of pH, ionic strength and surface coverage are strongly influenced by the magnitude of f. As a consequence, the CD model can fit adsorption data equally well with either an inner-sphere complex or both inner- and outer-sphere complexes (Rietra et al., 2001a), leading to a loss of sensitivity of the model to alternative speciation schemes. Even when both inner- and outer-sphere species are used, the predicted proportions of the two as a function of ionic strength may not agree with spectroscopic data (e.g. sulfate on goethite, Rietra et al., 2001a).

The recently developed dipole modification of the triple-layer model (ETLM, Sverjensky and Fukushi, 2006) is capable of independently predicting the proportions of inner- and outer-sphere surface complexes as functions of pH, ionic strength, and surface coverage consistent with spectroscopic results. This is possible because the ETLM takes into account a previously neglected phenomenon integral to ligand exchange reactions: the electrostatic work associated with desorption of water dipoles from a charged surface. It has been shown that the magnitude of the electrostatic work associated with this dipole modification to the TLM is substantial and depends only on the stoichiometry of the surface reaction. In contrast to the CD model, no new fitting parameters are involved. As a result, the sensitivity of the ETLM to predicting alternate speciation schemes is enhanced. When the structures of adsorbed anions established in spectroscopic studies are used to calibrate models of bulk adsorption data, the models then independently predict the proportions of inner- to

outer-sphere surface complexes as functions of pH, ionic strength and surface coverage. The predicted proportions compare very favorably with spectroscopic results for sulfate (SO_4^{2-}) on goethite (Peak et al., 1999; Wijnja and Schulthess, 2000), arsenite (AsO_3^{3-}) on β-Al(OH)$_3$ (Arai et al., 2001) and oxalate ($C_2O_4^{2-}$) on goethite (Persson and Axe, 2005). In addition, prediction of ζ-potentials is in qualitative agreement with electrokinetic data.

We start here with the ETLM description of inner- and outer-sphere As(III) species depicted in Fig. 1 (Sverjensky and Fukushi, 2006). The inner-sphere species is a bidentate, binuclear As(III) species represented by

$$2 >\mathrm{SOH} + \mathrm{As(OH)_3^0} = (>\mathrm{SO})_2\mathrm{As(OH)^0} + 2\mathrm{H_2O} \quad (1)$$

$${}^{*}\mathrm{K}^{\theta}_{(>\mathrm{SO})_2\mathrm{As(OH)^0}} = \frac{a_{(>\mathrm{SO})_2\mathrm{As(OH)^0}} a^2_{\mathrm{H_2O}}}{a^2_{>\mathrm{SOH}} a_{\mathrm{As(OH)_3^0}}} 10^{\frac{F(\Delta\psi_{r,1})}{2.303RT}} \quad (2)$$

The outer-sphere species is represented by

$$>\mathrm{SOH} + \mathrm{As(OH)_3^0} = >\mathrm{SOH_2^+\_AsO(OH)_2^-} \quad (3)$$

and

$${}^{*}\mathrm{K}^{\theta}_{>\mathrm{SOH_2^+\_AsO(OH)_2^-}} = \frac{a_{>\mathrm{SOH_2^+\_AsO(OH)_2^-}}}{a_{>\mathrm{SOH}} a_{\mathrm{As(OH)_3^0}}} 10^{\frac{F(\psi_0-\psi_\beta)}{2.303RT}} \quad (4)$$

In the equilibrium constants in Eqs. (2), (4), and subsequent equations, the superscript "*" represents a reaction relative to the species >SOH and the superscript "θ" represents site-occupancy standard states adopted in the present study (see Appendix A). In the exponential term of Eq. (2), $\Delta\psi_{r,1}$ represents the electrostatic factor related to the work done in an electric field when species in the reaction move on or off the charged surface. Traditionally, $\Delta\psi_{r,1}$ for an inner-sphere complex has been evaluated taking into account only the ions in the reaction. With the ETLM, $\Delta\psi_{r,1}$ is evaluated taking into account the ions and the water dipoles released in the reaction (see below). For the outer-sphere complex in Eq. (4), we continue to express the electrostatic factor in the traditional way for β-plane complexes in the TLM (Davis and Leckie, 1980).

The species and reactions shown in Fig. 1 have been applied to fitting the As(III) adsorption data for alumina depicted in Fig. 2a (Sverjensky and Fukushi, 2006). This enabled prediction of the pH and ionic strength dependence of the proportions of the two As(III) surface species shown in Figs. 2b–d. It can be seen in Figs. 2b and c that the relative importance of the outer-sphere species is predicted to increase with pH and to decrease with increasing ionic strength, which is consistent with experimental observations by Arai et al. (2001). In addition, it can be seen in Fig. 2d that the predicted proportions of outer- to inner-sphere species at pH 8 agrees closely with the XANES result from Arai et al. (2001).

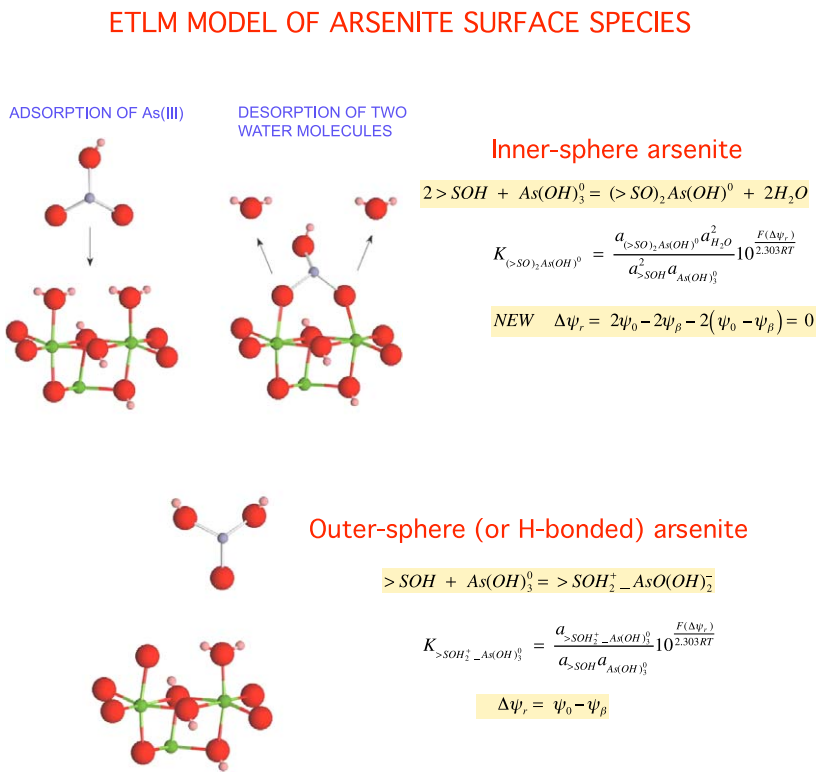

Fig. 1. Diagrammatic representations and model reactions of the formation of inner- and outer-sphere arsenite surface species on a fragment of the structure of aluminum or iron oxide according to the ETLM (Sverjensky and Fukushi, 2006). The inner-sphere species forms by a ligand-exchange reaction which releases two water dipoles. This effect is taken into account in the electrostatic term for the reaction ($\Delta\psi_r$), which includes contributions from the ions and the waters in the reaction. In contrast, the outer-sphere (or H-bonded) arsenite surface species has an electrostatic term dependent only on the ions in the reaction.

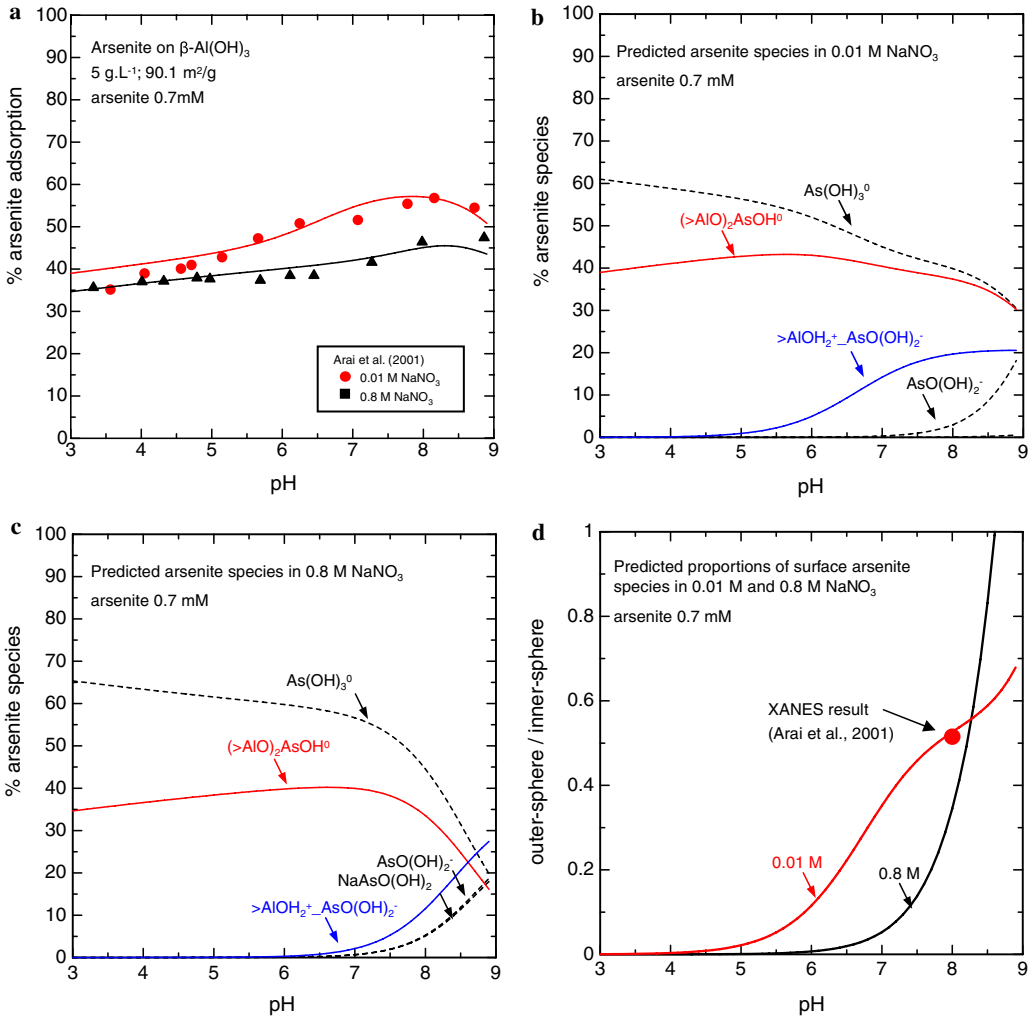

Fig. 2. As(III) adsorption on β-Al(OH)$_3$. The curves were calculated with the ETLM using the arsenite surface species and parameters in Tables 1 and 2. (a) As(III) adsorption as a function of pH and ionic strength. The curves represent regression fits of the experimental data plotted as symbols. (b–c) Predicted model arsenite surface and aqueous speciation. The proportion of outer-sphere complex increases with pH, but decreases with increasing ionic strength consistent with XANES results from Arai et al. (2001). (d) Predicted proportions of outer- to inner-sphere arsenite surface complexes at 0.01 and 0.8 M $NaNO_3$. The solid curve for 0.01 M agrees with the experimental XANES result at pH 8.

Reactions (1) and (3) are consistent with the X-ray spectroscopic results and the molecular calculations summarized above. In the calculations reported below, we investigate the applicability of the spectroscopically identified species to describe adsorption data under a range of conditions much wider than the spectroscopic studies. It is therefore a fundamental assumption that species identified on, for example, alumina, will also be found on iron oxides. It will be shown below that this assumption is reasonable for a wide range of conditions because the proportions of the inner- and outer-sphere species can vary sufficiently from one oxide to another to result in macroscopically different adsorption behavior. For some conditions, two additional reactions were needed to describe the macroscopic data. At high pH values, on ferrihydrite and am.FeO a deprotonated inner-sphere bidentate, binuclear species was added consistent with

$$2\,{>}\mathrm{SOH} + \mathrm{As(OH)_3^0} = (>\mathrm{SO})_2\mathrm{AsO^-} + \mathrm{H^+} + 2\mathrm{H_2O} \quad (5)$$

$$^{*}\mathrm{K}^{\theta}_{(>\mathrm{SO})_2\mathrm{AsO^-}} = \frac{a_{(>\mathrm{SO})_2\mathrm{AsO^-}}\, a_{\mathrm{H^+}}\, a^2_{\mathrm{H_2O}}}{a^2_{>\mathrm{SOH}}\, a_{\mathrm{As(OH)_3^0}}}\, 10^{\frac{F(\Delta\psi_{r,5})}{2.303RT}} \quad (6)$$

In the exponential term of Eq. (6), $\Delta\psi_{r,5}$ represents the electrostatic factor related to the work done in an electric field when species in the reaction move on or off the charged surface. As for $\Delta\psi_{r,1}$ mentioned above, the ETLM evaluation of $\Delta\psi_{r,5}$ takes into account the ions and the water dipoles released in the reaction. On HFO at extremely low surface coverages, an outer-sphere complex was needed, consistent with

$$2\,{>}\mathrm{SOH} + \mathrm{H^+} + \mathrm{As(OH)_3^0} = (>\mathrm{SOH_2^+})_2\_\mathrm{AsO(OH)_2^-} \quad (7)$$

and

$$^{*}\mathrm{K}^{\theta}_{(>\mathrm{SOH_2^+})_2\_\mathrm{AsO(OH)_2^-}} = \frac{a_{(>\mathrm{SOH_2^+})_2\_\mathrm{AsO(OH)_2^-}}}{a^2_{>\mathrm{SOH}}\, a_{\mathrm{H^+}}\, a_{\mathrm{As(OH)_3^0}}}\, 10^{\frac{F(2\psi_0-\psi_\beta)}{2.303RT}} \quad (8)$$

Both of the As(III) surface species in Eqs. (5) and (7) are also consistent with the X-ray results.

2.2. Water dipole desorption and the electrostatics of ligand exchange

Inner-sphere anion adsorption is thought to proceed by a ligand exchange mechanism involving release of one or more water dipoles (Zhang and Sparks, 1990; Stumm, 1992; Grossl et al., 1997). In order to show clearly how the electrostatics of this process is treated in the ETLM, we break up Eq. (1) into two reactions. First, a reaction in which surface sites are protonated and $As(OH)_3^0$ is adsorbed to the β-plane of the TLM, and deprotonated, can be represented

$$2 >SOH + 2H^+ + As(OH)_3^0 = (>SOH_2^+)_2\text{-}AsO_2(OH)^{2-} + 2H^+ \quad (9)$$

The adsorbed As(III) species is represented in the upper left panel of Fig. 1. In Eq. (9), the two protons on the left-hand side of the reaction react to form the positively charged surface sites and the two protons on the right-hand side are released from the adsorbed As-species. Clearly, the protons cancel in the reaction. They are retained here to show how the electrostatic factor is formulated.

The electrostatic factor associated with Eq. (9), $\Delta\psi_{r,9}$, is evaluated in the traditional way by

$$\Delta\psi_{r,9} = 2\psi_0 - 2\psi_\beta \quad (10)$$

where the term $2\psi_0$ refers to changes in the potential experienced by the $2H^+$ ions adsorbing to the 0-plane and the term $-2\psi_\beta$ refers to changes in the potential associated with the desorption of the $2H^+$ ions from the As-species on the β-plane.

In a second reaction, water is desorbed from the 0-plane and an inner-sphere complex is formed

$$(>SOH_2^+)_2\text{-}AsO_2(OH)^{2-} = (>SO)_2As(OH)^0 + 2H_2O \quad (11)$$

The inner-sphere As(III) and the release of the two waters is depicted in the upper right panel of Fig. 1. For Eq. (11), traditional surface complexation treatments of ligand exchange reactions have implicitly assumed that the electrostatic work is zero (Stumm, 1992; Hiemstra and van Riemsdijk, 1996), i.e. $\Delta\psi_{r,11} = 0$. However, the movement of dipolar molecules, such as water, to or from a charged surface does involve electrostatic work (Bockris and Reddy, 1970). The magnitude of the electrostatic work associated with desorption of n moles of water dipoles from the 0-plane in the ETLM is given by (Sverjensky and Fukushi, 2006)

$$\delta w \approx nF(\psi_0 - \psi_\beta) \quad (12)$$

where F represents the Faraday constant ($F = 96{,}485\ C\ mol^{-1}$), and ψ_0 and ψ_β represent the potentials at the 0- and β-planes of the TLM, respectively. Applying Eq. (12) to the reaction shown in Eq. (11), results in

$$\delta w_{11} \approx 2F(\psi_0 - \psi_\beta) \quad (13)$$

The electrostatic work of dipole desorption shown in Eq. (13) can be expressed in equilibrium constant form by

$$K_{11} = 10^{\frac{-2F(\psi_0 - \psi_\beta)}{2.303RT}} \quad (14)$$

i.e., the electrostatic factor for Eq. (11), $\Delta\psi_{r,11}$, is given by

$$\Delta\psi_{r,11} = -2(\psi_0 - \psi_\beta) \quad (15)$$

The overall reaction in Eq. (1) represents the sum of the reactions in Eqs. (9) and (11), so the overall electrostatic factor for Eq. (1), $\Delta\psi_{r,1}$, is given by the sum of Eqs. (10) and (15),

$$\text{i.e. } \Delta\psi_{r,1} = \Delta\psi_{r,9} + \Delta\psi_{r,11} = 2\psi_0 - 2\psi_\beta - 2(\psi_0 - \psi_\beta) = 0 \quad (16)$$

Similar reasoning for Eqs. (5) and (6) results in

$$\Delta\psi_{r,5} = 2\psi_0 - 3\psi_\beta - 2(\psi_0 - \psi_\beta) = -\psi_\beta \quad (17)$$

Eqs. (16) and (17) express changes in the potentials experienced by the $2H^+$ ions adsorbing to the 0-plane, the protons desorbing from the β-plane, and the $2H_2O$ desorbing from the 0-plane. Traditionally the electrostatic effects of the water dipole desorption have been ignored, but Eqs. (16) and (17) indicate the very large effect of the dipole modification to the TLM.

For Eq. (16), the electrostatic work associated with the movement of the ions to and from the surface is completely cancelled by the work associated with removing the water dipoles from the surface. As it happens, this result is the same, for modelling purposes, as if a 0-plane complex in the TLM had been used with the same stoichiometry as in Eq. (1). However, in Eq. (17), $\Delta\psi_r$ is not equal to zero (see also oxalate on goethite where $\Delta\psi_r = -\psi_\beta$, Sverjensky and Fukushi, 2006, and arsenate on hematite where $\Delta\psi_r = -\psi_\beta$, Arai et al., 2004). As a consequence, the ETLM predictions of adsorption as a function of pH, ionic strength and surface coverage, in general, are different from those of the TLM when the electrostatics of the water dipole were not considered.

In the calculations described below, the ETLM is used to regress a wide array of As(III) adsorption data. From a practical standpoint, the implementation of the ETLM differs only slightly from past use of the TLM. All surface protonation, electrolyte adsorption, and capacitance–potential–charge relations are as traditionally specified (e.g. Sverjensky, 2005). The only difference arises in the treatment of inner-sphere As(III) adsorption reactions where the electrostatic factor is specified differently (e.g. Eq. (16)). The resulting As(III) equilibrium constants referring to the hypothetical 1.0 M standard state are subsequently corrected to site occupancy standard states

so that they can be sensibly compared from one solid to another.

3. Application to arsenite adsorption

3.1. Aqueous speciation, surface protonation and electrolyte adsorption

3.1.1. Aqueous speciation model

Aqueous speciation calculations were carried out taking into account aqueous ionic activity coefficients appropriate to single electrolytes up to high ionic strengths calculated with the extended Debye-Huckel equation (Helgeson et al., 1981). Electrolyte ion pairs used were consistent with previous studies (Criscenti and Sverjensky, 1999, 2002). Aqueous As(III) protonation equilibria were taken from a recent study (Nordstrom and Archer, 2003):

$$As(OH)_3^0 = AsO(OH)_2^- + H^+; \quad \log K = -9.17 \tag{18}$$

$$AsO(OH)_2^- = AsO_2(OH)^{2-} + H^+; \quad \log K = -14.1 \tag{19}$$

$$AsO_2(OH)^{2-} = AsO_3^{3-} + H^+; \quad \log K = -15.0 \tag{20}$$

Of these, only the first deprotonation reaction is of importance under the conditions of the present study. Other aqueous As(III) species such as polymerized arsenic oxyhydroxy species (Tossell, 1997) and arsenic-carbonate species (Neuberger and Helz, 2005) are not significant under the conditions of the present study.

In the calculations summarized below, As(III) adsorption data were analysed over a wide range of ionic strengths (0.001–1.0) and pH values up to about 11. At the highest ionic strengths and pH values, it might be expected that anionic arsenic could form an aqueous complex with an abundant electrolyte cation such as Na^+. Based on analysis of the adsorption of As(III) on am.AlO from Goldberg and Johnston (2001) at pH values of 9–11 and ionic strengths up to 1.0, described below, the following reaction is proposed:

$$As(OH)_3^0 + Na^+ = NaAsO(OH)_2^0 + H^+; \quad \log K = -8.6 \tag{21}$$

It can be seen in the speciation diagrams below that this reaction is only important at ionic strengths greater than about 0.5. As a test of the validity of Eq. (21), it was included in all other calculations reported below. In all cases at high ionic strengths, the results helped to achieve consistency with measured adsorption data. Nevertheless, it is emphasized that the present results for Eq. (21) are model dependent and should be tested through additional experimental aqueous studies or molecular calculations.

3.1.2. Surface protonation and electrolyte adsorption parameters

An internally consistent set of surface protonation and electrolyte adsorption equilibrium constants, capacitances, and site densities are essential to the development of a predictive surface complexation model for As(III) on a range of different oxides. Unless the equilibrium constants for protonation and electrolyte adsorption refer to a consistent set of standard state assumptions, the As(III) equilibrium constants for different solids, or different samples of the same solid, cannot be sensibly compared, let alone placed on a predictive basis. A common source of inconsistency arises from failure to recognize that the hypothetical 1.0 molar standard state for surface species frequently adopted in surface complexation studies includes a dependence on site density and BET surface area. Equations for converting this standard state to site occupancy standard states independent of site density and surface area (Sverjensky, 2003; Sverjensky, 2006) are summarized in the Appendix A.

The surface protonation and electrolyte adsorption equilibrium constants used in the present study are summarized in Table 1. For convenience, these are given both for the site occupancy standard states, expressed by the superscript "θ", as well as the often used hypothetical 1.0 molar standard state, expressed by the superscript "$*$". The surface protonation constants referring to the site occupancy standard states were calculated from values of pH_{ZPC} and ΔpK_n^θ using theoretically predicted values of ΔpK_n^θ. Values of pH_{ZPC} were taken from the experimental studies that report the As(III) adsorption, preferably using low ionic strength isoelectric points or, where these were not available, point-of-zero-salt effects corrected for electrolyte adsorption (Sverjensky, 2005). For magnetite, goethite and HFO (Dixit and Hering, 2003), neither isoelectric points nor surface titration data were reported for the samples used in the As(III) study. Values of pH_{ZPC} for magnetite and goethite were predicted for the present study using Born solvation and crystal chemical theory (Table 1). For HFO, this was not possible because the predictions require a value of the dielectric constant of the solid, which has not been established because it has such poor crystallinity. Instead, it was assumed that this HFO has the same surface properties as those measured in an earlier study (Davis and Leckie, 1978) for which the $pH_{ZPC} = 7.9$ and the surface area was equal to 600 $m^2\ g^{-1}$. As will be seen below, when the As(III) equilibrium constants are compared, these proved to be very reasonable assumptions.

It should be emphasized that not all poorly crystalline or amorphous iron oxides behave identically. We use here the nomenclature for each oxide given by the original authors. For example, the amorphous iron oxide (am.FeO) in Table 1 (Goldberg and Johnston, 2001) has a $pH_{ZPC} = 8.5$ from electrophoretic mobility measurements, which is significantly larger than that for the type of HFO studied by Davis and Leckie (1978). In order to be able to build such fundamental differences into a predictive model, it was assumed here that the different pH_{ZPC} values for the HFO and am.FeO could be accounted for in the context of Born solvation and crystal chemical theory (Sverjensky, 2005). Using the theoretical equation for pH_{ZPC} as a function of dielectric constant given in Sverjensky (2005), and assuming that HFO and am.FeO have the same average Pauling Bond strength per angstrom, effective dielectric

Table 1
Sample characteristics, surface protonation and electrolyte adsorption equilibrium constants, and capacitances used in generating the equilibrium constants for As(III)

Solid[c]	N_s[d] (nm^{-2})	A_s[e] ($m^2\ g^{-1}$)	C_s ($g\ L^{-1}$)	pH_{ZPC}[f]	ΔpK_n^{θ}[g]	C_1[h] ($\mu F\ cm^{-2}$)	SALT (mL)	$\log K_1^{\theta}$	$\log K_2^{\theta}$	$\log K_{M^+}^{\theta}$	$\log K_{L^-}^{\theta}$	$\log {}^*K_1^0$	$\log {}^*K_2^0$	$\log {}^*K_{M^+}^0$	$\log {}^*K_{L^-}^0$
β-$Al(OH)_3$	5.0	90.1	5.0	9.3	5.6	60	NaCl	6.5	12.1	2.9	2.7	5.8	−12.8	−9.9	8.5
Fe_3O_4	3.0	90.0	0.5	6.9	5.7	131	$NaClO_4$	4.05	9.75	3.4	2.1	3.6	−10.2	−6.8	5.7
FeOOH	3.5	54.0	0.5	9.2	5.6	120	$NaClO_4$	6.4	12.0	3.4	2.4	6.1	−12.3	−8.9	8.5
HFO	3.8	600	0.03	7.9	5.6	100	$NaClO_4$	5.1	10.7	4.3[i]	4.5[i]	3.7	−12.1	−7.8	8.2
Ferrihydrite	3.8	600	2.0	8.5	5.6	110	NaCl	5.7	11.3	4.0[j]	4.0[j]	4.3	−12.7	−8.7	8.3
am.FeO	3.8	600	4.0	8.5	5.6	110	NaCl	5.7	11.3	4.0[k]	4.0[k]	4.3	−12.7	−8.7	8.3
am.FeO	3.8	600	0.5	8.5	5.6	110	NaCl	5.7	11.3	4.0[k]	4.0[k]	4.3	−12.7	−8.7	8.3
am.AlO	2.5	600	4.0	9.4	5.6	160	NaCl	6.6	12.2	3.1	2.7	5.4	−13.4	−10.3	8.1
α-$Al(OH)_3$	3.0	13	20.0	8.7	5.6	140	$NaNO_3$	5.9	11.5	2.6[l]	2.4[l]	6.3	−11.1	−8.5	8.7

Values of $\log K_1^{\theta}$, $\log K_2^{\theta}$, $\log K_{M^+}^{\theta}$ and $\log K_{L^-}^{\theta}$ refer to site-occupancy standard states for the reactions listed below[a]. Values of $\log K_1^{\theta}$ and $\log K_2^{\theta}$, were predicted using the given values of pH_{ZPC} and ΔpK_n^{θ}. Values of $\log K_{M^+}^{\theta}$ and $\log K_{L^-}^{\theta}$ were taken from published theoretical predictions (Sverjensky, 2005) unless otherwise noted. Values of $\log K_1^0$, $\log K_2^0$, $\log {}^*K_{M^+}^0$ and $\log {}^*K_{L^-}^0$ refer to the hypothetical 1.0 M standard state and the reactions listed below[b]. They were calculated from the values of $\log K_1^{\theta}$, $\log K_2^{\theta}$, $\log K_{M^+}^{\theta}$ and $\log K_{L^-}^{\theta}$ with the aid of Eqs. (A.3), (A.4), (A.15) and (A.16) using the tabulated values of N_s, A_s, pH_{ZPC} and ΔpK_n^{θ}.

[a] $\log K_1^{\theta}$: $>SOH + H^+ = >SOH_2^+$; $\log K_2^{\theta}$: $>SO^- + H^+ = >SOH$; $\log K_{M^+}^{\theta}$: $>SO^- + M^+ = >SO^-\_M^+$; $\log K_{L^-}^{\theta}$: $>SOH_2^+ + L^- = >SOH_2^+\_L^-$.

[b] $\log {}^*K_1^0$: $>SOH + H^+ = >SOH_2^+$; $\log {}^*K_2^0$: $>SO^- + H^+ = >SOH$; $\log {}^*K_{M^+}^0$: $>SOH + M^+ = >SO^-\_M^+ + H^+$; $\log {}^*K_{L^-}^0$: $>SOH + H^+ + L^- = >SOH_2^+\_L^-$.

[c] β-$Al(OH)_3$ (Arai et al., 2001); Fe_3O_4, FeOOH, and HFO (Dixit and Hering, 2003); ferrihydrite (Jain et al., 1999a,b); am.FeO and am.AlO (Goldberg and Johnston, 2001); α-$Al(OH)_3$ (Weerasooriya et al., 2003).

[d] Values generated by regression of As(III) adsorption as a function of surface coverage (see text). Where no data as a function of surface coverage were available, e.g., β-$Al(OH)_3$ and am.AlO, values for N_s were assigned based on regression of arsenate adsorption data which were sensitive to the selection of site density.

[e] Surface areas from BET measurements by the authors cited in c. with the exception of HFO, ferrihydrite, am.FeO, and am.AlO for which the surface area was taken from the study of hydrous ferric hydroxide by Davis and Leckie (1978).

[f] Zero points of charge taken from measured low ionic strength isoelectric points for β-$Al(OH)_3$ (Arai et al., 2001) and am.FeO and am.AlO (Goldberg and Johnston, 2001). Values for Fe_3O_4 and FeOOH are predicted (Sverjensky, 2005). The value for HFO was assumed to be the same as measured by Davis and Leckie (1978). The value for α-$Al(OH)_3$ represents a value of pH_{PZSE} (Weerasooriya et al., 2003) corrected for electrolyte effects after Sverjensky (2005).

[g] Predicted theoretically (Sverjensky, 2005).

[h] Predicted theoretically (Sverjensky, 2005) except for α-$Al(OH)_3$ and ferrihydrite where C_1 values were obtained by regression of surface charge data given by Weerasooriya et al. (2003) and Jain et al. (1999a,b), respectively. The value of C_1 for am.FeO was set equal to that for ferrihydrite.

[i] Calculated from the results of regression by Criscenti and Sverjensky (2002) of *HFO* proton surface charge data from Davis and Leckie (1978).

[j] Calculated from the results of regression of proton surface charge data in the present study (Fig. 6).

[k] Assumed equal to the results for ferrihydrite because am.FeO has the same $pH_{ZPC} = 8.5$.

[l] Obtained by regression of surface charge data given by Weerasooriya et al. (2003).

constants of 1000 and 32 were estimated for HFO and am. FeO, respectively (Table 2). The large dielectric constant for HFO relative to the am.FeO is surprizing, but it will be shown below that this is consistent with the large differences between the As(III) equilibrium constants on these two solids. Because the ferrihydrite in Tables 1 and 2 has the same pH_{ZPC} as the am.FeO, its dielectric constant was also set to 32. A similar approach was used for am. AlO and β-$Al(OH)_3$. Although the dielectric constants obtained in this way are subject to substantial uncertainty, they provide a basis for testing whether the differences in the As(III) adsorption equilibrium constants for these solids can also be accounted for with Born solvation theory (see below). The physical reason for the differences between these two forms of hydrous iron oxide cannot be established without a more detailed experimental characterization of the solids.

The surface protonation and electrolyte adsorption equilibrium constants in Table 1 referring to the hypothetical 1.0 molar standard state were calculated from the equilibrium constants for the site occupancy standard states using theoretical relations (Appendix A) involving the surface areas and site densities of the actual samples (Table 1). With the exception of HFO, ferrihydrite, am.FeO, and am.AlO, for which it was assumed that the surface area is 600 $m^2\ g^{-1}$, all the surface areas in Table 1 come from BET measurements. However, the site densities in Table 1 were derived from regression of the As(III) adsorption data as a function of surface coverage (with two exceptions, β-$Al(OH)_3$ and am.AlO, as noted in Table 1). With very wide ranges of surface coverage, obtaining site densities from regression necessitates considerable care because at high enough surface coverages, As(III) may adsorb to different sites or it may accumulate through surface processes other than adsorption alone. For example, studies of hydrous ferric oxide have noted that high surface coverages of As(III), about $10^{-5.0}$ mol As(III) m^{-2} (Raven et al., 1998), may be caused by surface precipitation or surface polymerization (Raven et al., 1998; Jain et al., 1999b; Stanforth, 1999; Jain and Loeppert, 2000; Dixit and Hering, 2003). An additional possible process is diffusion into the structure. However, the transition from adsorption to these additional surface processes has not been well documented. It may occur somewhere between about $10^{-5.9}$ and $10^{-5.0}$ mol As(III) m^{-2} (Raven et al., 1998). Under these circumstances it is appropriate to adopt the simplest approach for generating a site density. In the present study, emphasis has been placed on obtaining site densities by regression of the lowest available surface coverages and extrapolating these results to obtain an estimate of the upper limit of surface coverage for the validity of the adsorption model.

3.2. Adsorption of As(III) on magnetite from Dixit and Hering (2003)

The solid curves in Figs. 3a and b represent regression calculations using the same species as in Fig. 1, i.e. the inner-sphere species $(>FeO)_2As(OH)^0$ and the outer-sphere species $>FeOH_2^+\_AsO(OH)_2^-$ in Eqs. (1) and (3) together with the parameters summarized in Tables 1 and 2. It should be emphasized that the choice of the inner-sphere and the outer-sphere As(III) surface species is based on the EXAFS and XANES results for As(III) on β-$Al(OH)_3$ (Arai et al., 2001). The state of protonation of these species is based on the fact that Eqs. (1) and (3) provided a close fit to the adsorption data for As(III) on β-$Al(OH)_3$ as a function of pH and ionic strength, as well as prediction of the relative proportions of the inner- and outer-sphere surface species consistent with the XANES data as described previously (Sverjensky and Fukushi, 2006). It can be seen in Fig. 3a that the calculated curves provide a close description of the magnetite adsorption data over a wide range of pH and a factor of three of surface coverage in 0.01 M $NaClO_4$ solutions. At surface coverages above about $10^{-5.7}$ mol As(III) m^{-2}, it can be seen in Fig. 3b that the model systematically underestimates the amount of adsorbed arsenic. Based on the discussion above, it seems likely that the highest surface coverages in Fig. 3b reflect processes operating in addition to adsorption, such as surface precipitation, polymerization, or diffusion into the structure. Further experimental characterization of the high surface coverages is required to understand the nature of As(III) uptake under these conditions.

The predicted model speciation of As(III) on the surface of the magnetite is shown in Figs. 3c–e. Speciation plots are given for the lowest and highest surface coverages from Fig. 3a in 0.01 M $NaClO_4$ solutions, as well as a prediction for 0.1 M $NaClO_4$ solutions. For the lowest surface coverage, it can be seen in Fig. 3c that the outer-sphere species is predicted to predominate at pH values from about 5 to 10. In Figs. 3d and e, at increased surface coverage and higher ionic strength, the outer-sphere species still predominates at pH values from about 7 to 10. This contrasts with the situation for As(III) on β-$Al(OH)_3$ in Fig. 2 (and a number of other oxides, see below) where the outer-sphere species is predicted to be much less important than the inner-sphere complex under many conditions. The importance of the outer-sphere complex for the overall adsorption of As(III) on magnetite can be seen in Fig. 3a at pH values of 8–10. Under these conditions, the overall adsorption of As(III) is at a maximum because of the increased abundance of the outer-sphere species. In this regard, the results in Figs. 2 and 3 are similar: the overall arsenic adsorption increases with pH because of the increasing importance of the outer-sphere complex.

3.3. Adsorption of As(III) on goethite from Dixit and Hering (2003)

The solid curves in Figs. 4a and b again represent regression calculations using the inner-sphere species $(>FeO)_2As(OH)^0$ and the outer-sphere species $>FeOH_2^+\_AsO(OH)_2^-$ (Tables 1 and 2). In contrast to the data for magnetite, the data for goethite can be closely

Table 2
Equilibrium constants for As(III) adsorption from regression of the data in Figs. 1–7

Solid	ε_s[c]	$\log {}^*K^0_{(>SO)_2As(OH)^0}$	$\log {}^*K^0_{>SOH_2^+\_AsO(OH)_2^-}$	C_s (g L^{-1})	$\log K^\theta_{(>SO)_2As(OH)^0}$	$\log K^\theta_{>SOH_2^+\_AsO(OH)_2^-}$
β-Al(OH)$_3$	10.3[d]	5.0	3.1	5.0	−4.0	−2.8
Fe_3O_4	1000	7.5	4.4	0.5	2.0	0.8
FeOOH	15	9.3	3.8	0.5	−1.2	−2.3
HFO[e]	1000[d]	8.9	4.8	0.03	1.9	1.1
HFO[e]	1000[d]	9.7	4.8	0.0044	1.9	1.1
Ferrihydrite[f]	32[d]	6.8	3.7	2.0	0.4	−0.6
am.FeO	32[d]	5.6	3.3	4.0	−0.5	−1.0
am.FeO	32[d]	6.5	3.3	0.5	−0.5	−1.0
am.AlO	10.3[d]	4.0	3.2	4.0	−4.2	−2.2
α-Al(OH)$_3$	8.4	5.55	2.0	20.0	−3.8	−4.3

Values of $\log {}^*K^0_{(>SO)_2As(OH)^0}$ and $\log {}^*K^0_{>SOH_2^+\_AsO(OH)_2^-}$ refer to the hypothetical 1.0 M standard state and reactions formed from >SOH[a]. Values of $\log K^\theta_{(>SO)_2As(OH)^0}$ and $\log K^\theta_{>SOH_2^+\_AsO(OH)_2^-}$ refer to site-occupancy standard states for As(III) adsorption reactions[b] calculated from the values of $\log {}^*K^0_{(>SO)_2As(OH)^0}$ and $\log {}^*K^0_{>SOH_2^+\_AsO(OH)_2^-}$ with the aid of Eqs. (22) and (23) using values of N_s, A_s, C_s, pH_{ZPC} and ΔpK^θ_n from Table 1. Dielectric constants of the solids were used to plot $\log K^\theta_{(>SO)_2As(OH)^0}$ and $\log K^\theta_{>SOH_2^+\_AsO(OH)_2^-}$ in Fig. 10.

[a] $\log {}^*K^0_{(>SO)_2As(OH)^0}$: $2 > SOH + As(OH)^0_3 = (>SO)_2As(OH)^0 + 2H_2O$; $\log {}^*K^0_{>SOH_2^+\_AsO(OH)_2^-}$: $> SOH + As(OH)^0_3 => SOH_2^+\_AsO(OH)_2^-$.

[b] $\log K^\theta_{(>SO)_2As(OH)^0}$: $2 > SOH_2^+ + As(OH)^0_3 = (>SO)_2As(OH)^0 + 2H^+ + 2H_2O$; $\log K^\theta_{>SOH_2^+\_AsO(OH)_2^-}$: $> SOH_2^+ + As(OH)^0_3 => SOH_2^+\_AsO(OH)_2^- + H^+$.

[c] Solid dielectric constant (Sverjensky, 2005) unless otherwise noted.

[d] Values estimated with the aid of the theoretical equation relating pH_{ZPC} and $\frac{1}{\varepsilon_s}$ (Sverjensky, 2005) using values of the pH_{ZPC} equal to 7.9 (HFO), 8.5 (am.FeO and ferrihydrite), 9.4 (am.AlO), and 9.3 (β-Al(OH)$_3$).

[e] HFO at 0.03 g L^{-1} (Dixit and Hering, 2003), HFO at 0.0044 g L^{-1} (Wilkie and Hering, 1996). For both HFO an additional reaction was incorporated into the model (see text): $2 > SOH + H^+ + As(OH)^0_3 = (>SOH_2^+)_2\_AsO(OH)_2^-$, for which $\log {}^*K^0_{(>SOH_2^+)_2\_AsO(OH)_2^-} = 18.4$ and 19.2 for Dixit and Hering (2003) and Wilkie and Hering (1996), respectively. Taking into account the different solid concentrations, these results were reexpressed as the reaction $2 > SO^- + 3H^+ + As(OH)^0_3 = (>SOH_2^+)_2\_AsO(OH)_2^-$, resulting in $\log K^\theta_{(>SOH_2^+)_2\_AsO(OH)_2^-} = 11.4$.

[f] For ferrihydrite and am.FeO, an additional reaction was incorporated into the model (see text): $2 > SOH + As(OH)^0_3 = (>SO)_2AsO^- + H^+ + 2H_2O$, for which $\log {}^*K^0_{(>SO)_2AsO^-} = 3.0$ and −0.5 (at 4 g L^{-1}), respectively. These results were reexpressed as the reaction $2 > SO^- + H^+ + As(OH)^0_3 = (>SO)_2AsO^- + 2H_2O$, resulting in $\log K^\theta_{(>SO)_2AsO^-} = -3.4$ and −6.6, respectively.

fit using only the inner-sphere species in Eq. (1). The outer-sphere species was included in the model solely to place an upper limit on its importance under the experimental conditions studied by Dixit and Hering (2003). Consequently, the value of $\log {}^*K^0_{outer}$ for goethite in Table 1 represents merely an upper limit. The predicted dominance of the inner-sphere species on goethite is consistent with the EXAFS studies of As(III) on goethite in which an inner-sphere bidentate–binuclear species was reported (Manning et al., 1998; Farquhar et al., 2002). It can be seen in Figs. 4a and b that the calculated curves provide a close description of the adsorption data over a wide range of pH and surface coverages up to about $10^{-5.5}$ mol As(III) m^{-2} in 0.01 M $NaClO_4$ solutions. The data and calculations in Fig. 4b suggest a lack of surface precipitation, polymerisation, or diffusion under these conditions.

The predicted model speciation of As(III) on the surface of goethite is given in Figs. 4c–e. Speciation plots are given for the lowest and highest surface coverages in the 0.01 M $NaClO_4$ solutions studied by Dixit and Hering (2003), as well as a prediction of the surface speciation in 0.001 M $NaClO_4$ solutions. Inclusion of the outer-sphere species in the overall model permitted investigation of the possible importance of this species under conditions not accessed experimentally. The results shown in Figs. 4c–e are representative of the fact that at all conditions investigated, the inner-sphere species is predicted to predominate on goethite. The present calculations indicate that any outer-sphere As(III) species on goethite would be present at concentrations less than about 10% of the inner-sphere concentrations, which may be too low to be detected by current X-ray methods. It can be seen in Figs. 3 and 4 that the dominance of the inner-sphere complex for goethite compared to magnetite results in a different shape for the overall adsorption curves of As(III) on goethite compared to those for magnetite.

3.4. Adsorption of As(III) on HFO from Dixit and Hering (2003) and Wilkie and Hering (1996)

Freshly prepared (less than one day old) hydrous ferric oxide (HFO) was used in both studies referred to in Fig. 5. The results for extremely low surface coverages are depicted in Fig. 5a and those for moderate to higher surface coverages in Fig. 5b. The consistency between the two datasets can be seen in the isotherm in Fig. 5c. The six solid points in Fig. 5c represent the amounts adsorbed at pH 8 in Figs. 5a and b. The open symbols (also represented separately by Dixit and Hering, 2003) possibly represent surface precipitation or polymerization (Jain et al., 1999a,b; Dixit and Hering, 2003). The data depicted in Figs. 5a–c consequently represent a consistent dataset extending over an unusually wide range of surface coverages. The solid curves in Figs. 5a–c represent regression calculations using the inner- and outer-sphere As(III) species in Eqs. (1) and (3) (Tables 1 and 2), supplemented with Eq. (7) which be-

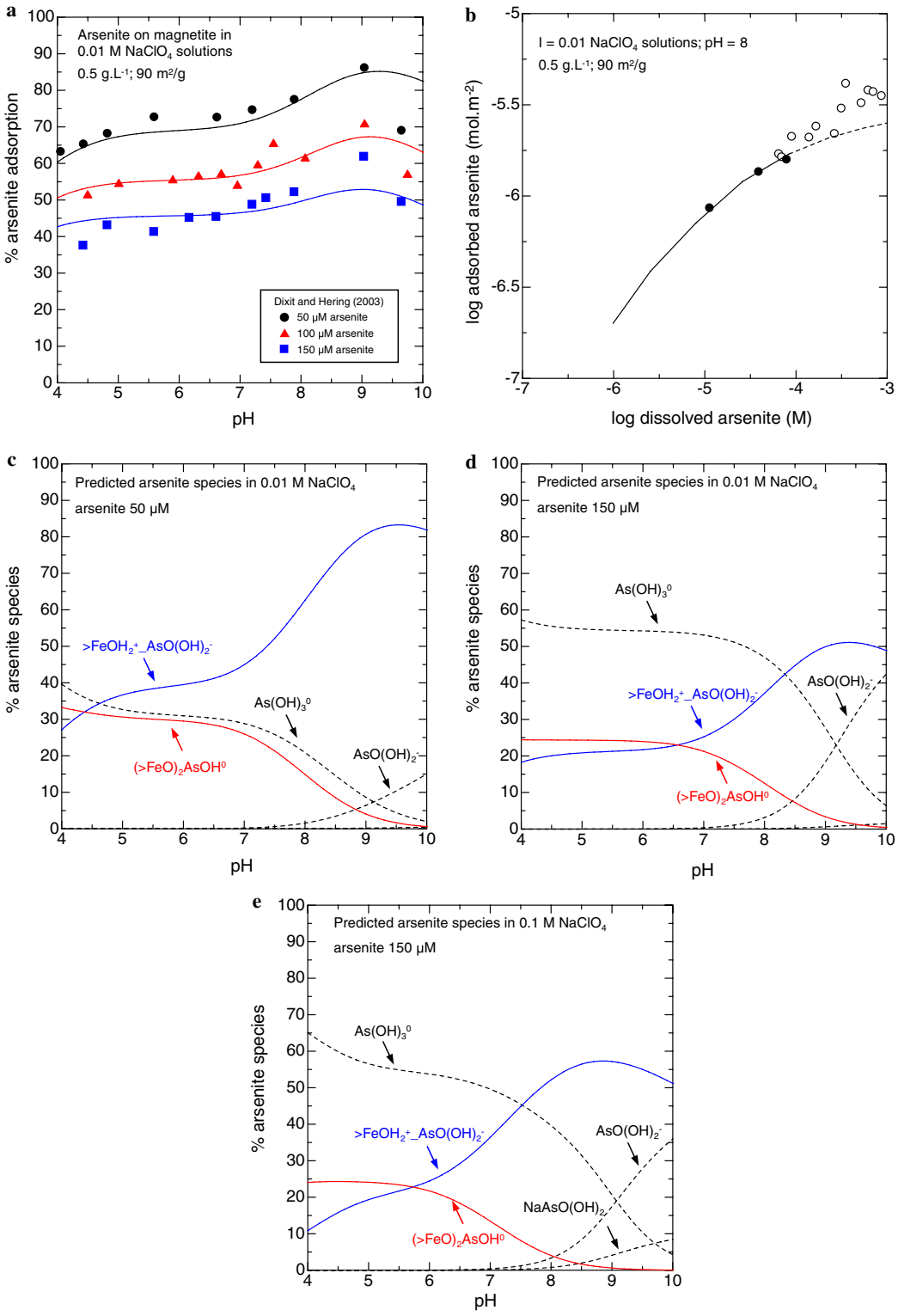

Fig. 3. As(III) adsorption on magnetite. The curves were calculated with the ETLM using the arsenite surface species and parameters in Tables 1 and 2. (a,b) As(III) adsorption as a function of pH, ionic strength and surface coverage. The curves represent regression fits of the experimental data plotted as symbols. (c–e) Predicted model arsenite surface and aqueous speciation.

came important at the lowest surface coverages. In contrast to the data for goethite, the data for HFO can only be closely fit using a combination of inner- and outer-sphere species. It can be seen in Figs. 5a and b that the calculated curves provide a close description of the adsorption data over a wide range of pH and surface coverages up to about $10^{-5.6}$ mol As(III) m^{-2} in 0.01 M $NaClO_4$ solutions. At surface coverages above about $10^{-5.6}$ mol As(III) m^{-2}, it can

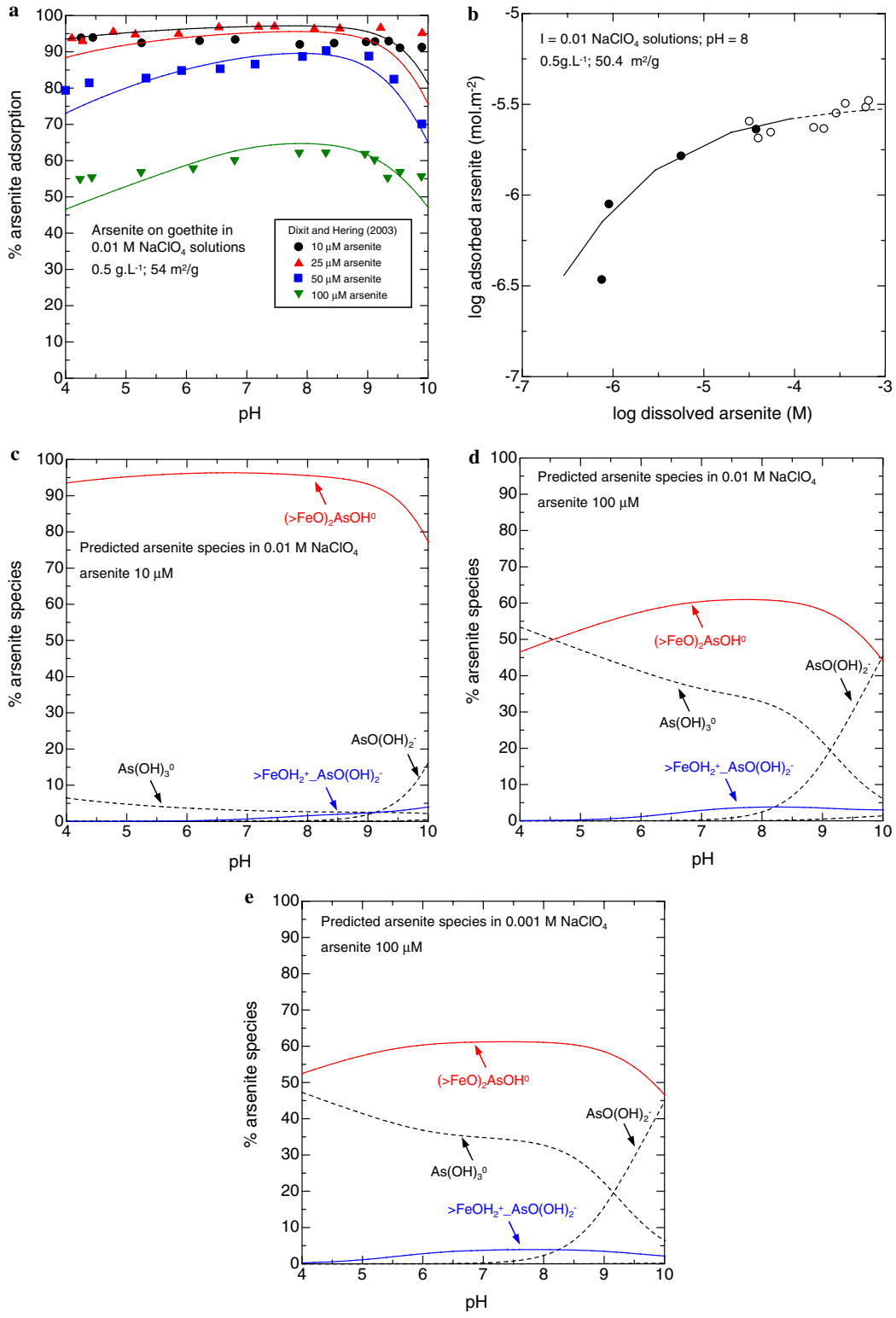

Fig. 4. As(III) adsorption on goethite. The curves were calculated with the ETLM using the arsenite surface species and parameters in Tables 1 and 2. (a,b) As(III) adsorption as a function of pH, ionic strength and surface coverage. The curves represent regression fits of the experimental data plotted as symbols. (c–e) Predicted model arsenite surface and aqueous speciation.

be seen in Fig. 5c that the model systematically underestimates the amount of adsorbed arsenic, as for magnetite, possibly because of the surface precipitation, polymerization, or diffusion referred to above.

The predicted model speciation of As(III) on the surface of HFO is given in Figs. 5d–f for the lowest though the highest surface coverages of Figs. 5a and b in the 0.01 M $NaNO_3$ and $NaClO_4$ solutions studied by Wilkie and Her-

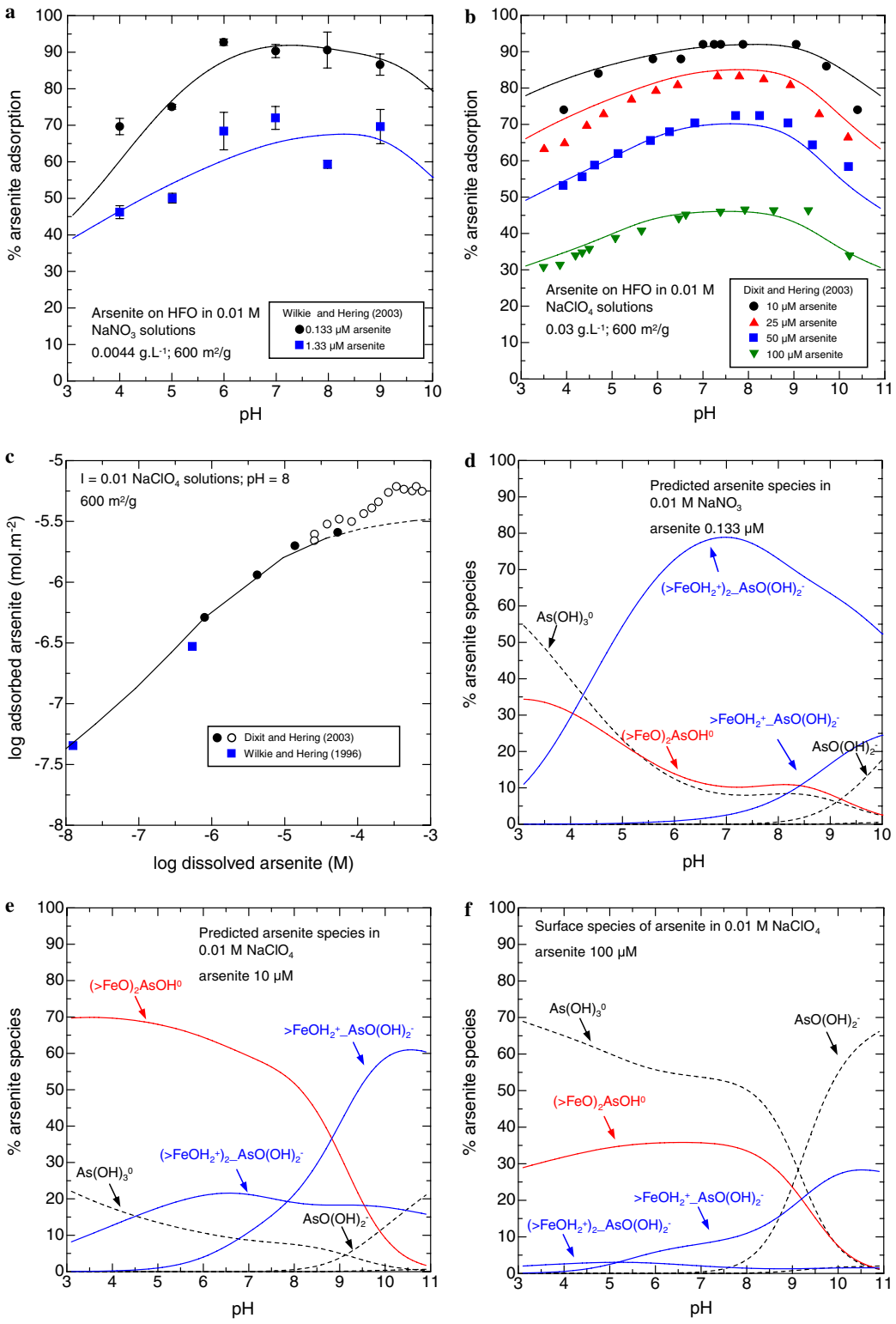

Fig. 5. As(III) adsorption on HFO. The curves were calculated with the ETLM using the arsenite surface species and parameters in Tables 1 and 2. (a–c) As(III) adsorption as a function of pH, ionic strength and surface coverage. The curves represent regression fits of the experimental data plotted as solid symbols. (d–f) Predicted model arsenite surface and aqueous speciation as a function of arsenite level.

ing (1996) and Dixit and Hering (2003). It can be seen that both inner- and outer-sphere As(III) species are important for HFO. At the lowest surface coverages (Fig. 5d), the binuclear outer-sphere species predominates from pH 4 to 10. However, at higher surface coverages (Figs. 5e and f), this species becomes unimportant. Instead the inner-sphere species predominates at pH values less than about 9 or 10, above which the mononuclear outer-sphere com-

plex predominates. Under the conditions of Figs. 5e and f, the behavior of HFO is intermediate to that of magnetite and goethite discussed above.

3.5. Adsorption of As(III) on ferrihydrite from Jain et al. (1999a,b) and Jain and Loeppert (2000)

The solid curves in Figs. 6a–d represent regression calculations using the inner- and outer-sphere As(III) species in Eqs. (1), (3), and (5) and the parameters in Tables 1 and 2. It should be emphasized that the types of data depicted in these figures are distinct from the other sets of data regressed in the present study because they include proton surface charge in the absence and the presence of arsenic (Figs. 6a and b) and proton coadsorption with arsenic at two fixed pH values (Fig. 6c), as well as the %As adsorbed (Fig. 6d). The data in Figs. 6b and c are particularly useful for constraining the protonation states of the As(III) surface species. The inclusion of the deprotonated inner-sphere complex in the model was essential for a description of the data in Fig. 6b. Only data represented by the solid symbols were regressed. Data at higher surface coverages presumably represent processes additional to adsorption, such as surface polymerization (Jain et al., 1999a,b; Jain and Loeppert, 2000). Uncertainties in the data depicted in Figs. 6a–d are difficult to assess, because they are not discussed in the original papers. With the exception of very low pH values in Fig. 6b, the solid curves represent a reasonable fit to the data.

The predicted model speciation of As(III) on the surface of this ferrihydrite is given in Figs. 6e and f for two surface coverages at $I = 0.1$ M. In contrast to the speciation depicted in Fig. 5, it can be seen here that the two inner-sphere As(III) species are overwhelmingly dominant for this ferrihydrite. As expected from the reaction stoichiometries, the protonated species dominates at low pH values and the deprotonated species at high pH values.

3.6. Adsorption of As(III) on amorphous iron oxide (am.FeO) from Goldberg and Johnston (2001)

As in the case of the ferrihydrite discussed above, the solid curves in Fig. 7a represent regression calculations using the inner- and outer-sphere As(III) species in Eqs. (1), (3), and (5) and the parameters in Tables 1 and 2. It can be seen in Fig. 7a that the calculated curves provide a close description of most of the adsorption data over a wide range of pH, surface coverage, and ionic strength in 0.01–1.0 M NaCl solutions. The addition of the deprotonated complex was found useful to account for adsorption at the higher pH values (pH > 9) and the lowest ionic strengths ($I = 0.01$) for both solid concentrations. Some systematic discrepancies are still apparent for the highest ionic strength (1.0 M) at low solid concentrations. This could be attributable to an inadequacy of the electrolyte model parameters. It should be noted that the surface protonation and electrolyte adsorption parameters used for this am. FeO were taken to be the same as those derived from the proton titration data given in Fig. 6a because the isoelectric points for the two solids are the same (Table 1).

Because the present model is a triple-layer model, it can be used to make predictions of the shift in the isoelectric point with arsenic loading, which can be compared with experimental electrokinetic results (Davis and Kent, 1990). This is an extremely severe test for a surface complexation model, rarely used, because it depends on the assumption that $\psi_d = \zeta$, and calculated values of ψ_d are very sensitive to model speciation schemes. For the am.-FeO, the experimental mobility data (Goldberg and Johnston, 2001) show some scatter and the uncertainties in the isoelectric points are probably about ±0.3 pH units. The isoelectric points are 8.5 (no arsenic), 8.8 (0.01 mM As) and 6.4 (1 mM As). Under the same conditions, the isoelectric point is predicted to shift strongly from 8.5 to 5.4 and 4.1. These shifts are at least in agreement with the direction of the shift for the highest As loading, but the overall predicted shift is too large. Considering that the predicted shifts are extremely sensitive to the abundance of the deprotonated binuclear bidentate inner-sphere complex, without this species the predicted shifts are too small, further attempts to more closely match the electrokinetic data were not pursued.

The predicted model speciation of As(III) on the surface of am.FeO is given in Figs. 7b–d for $I = 0.01$ and 1.0 for 4 g/L and $I = 1.0$ for 0.5 g/L, conditions studied by Goldberg and Johnston (2001). It can be seen that the two inner-sphere As(III) species dominate, except at the highest pH values and ionic strengths. The outer-sphere complex predominates only at pH values greater than about 9 at $I = 1.0$ for the surface coverages shown in these figures. These results are consistent with the inferences about surface species on am.FeO drawn from FTIR study by Goldberg and Johnston (2001) who suggested that inner-sphere species exist at pH 5 and that significant differences in the surface speciation are apparent at pH 10.

3.7. Adsorption of As(III) on amorphous aluminum oxide (am.AlO) from Goldberg and Johnston (2001)

The solid curves in Fig. 8a represent regression calculations using the inner- and outer-sphere species in Eqs. (1) and (3) (Tables 1 and 2). Both the inner- and outer-sphere species are required to fit the data in Fig. 8a. It can also be seen in Fig. 8a that the adsorption decreases very sharply at pH values above 9, and that the ionic strength dependence of the data diminishes. It is under these conditions that $As(OH)_3^0$ deprotonates (Eq. (18)). In order to adequately take this feature of the data into account, the aqueous species $NaAsO(OH)_2^0$ was added to the model with Eq. (21). With the exception of some of the data in Fig. 8a at pH values of 4–8 at 0.1 and 1.0 M, it can be seen that the calculated curves provide a close description of most of the adsorption data over a wide range of pH and ionic

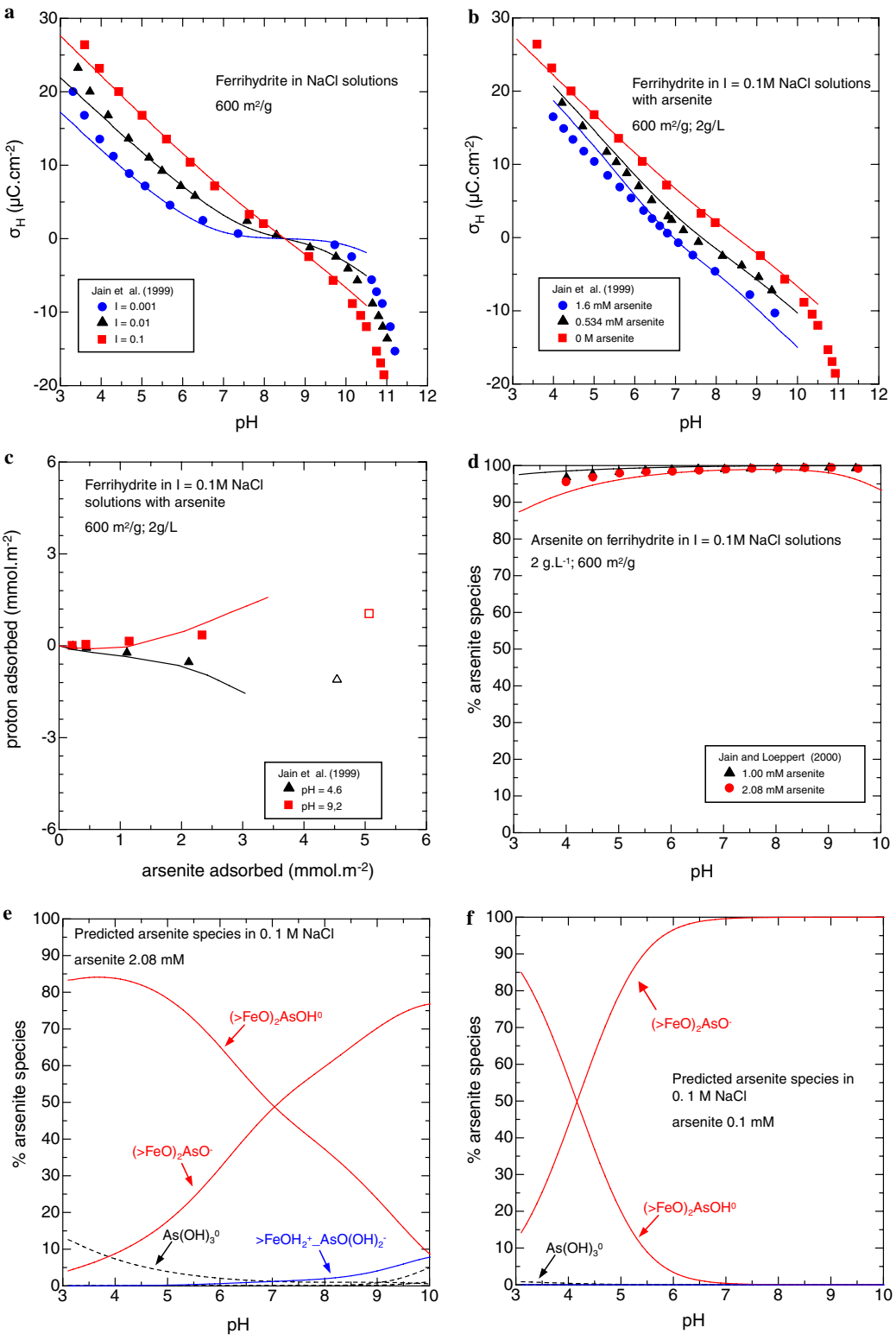

Fig. 6. As(III) adsorption on ferrihydrite. The curves were calculated with the ETLM using the arsenite surface species and parameters in Tables 1 and 2. The curves in (a–d) represent regression fits of the experimental data plotted as symbols. (a,b) Proton surface titration as a function of pH and ionic strength without arsenic (a) and with arsenic (b). (c) Proton co-adsorption with arsenic loading. (d) As(III) adsorption as a function of pH at 0.1 M electrolyte. (e,f) Predicted model arsenite surface and aqueous speciation.

strength. Also, as described above, the inclusion of this species is consistent with all the calculations at high pH values and high ionic strengths (e.g. Figs. 2, 7 and 9a).

As for the am.FeO above, predictions of the shift in the isoelectric point of am.AlO with arsenic loading can be compared with experimental electrokinetic results from

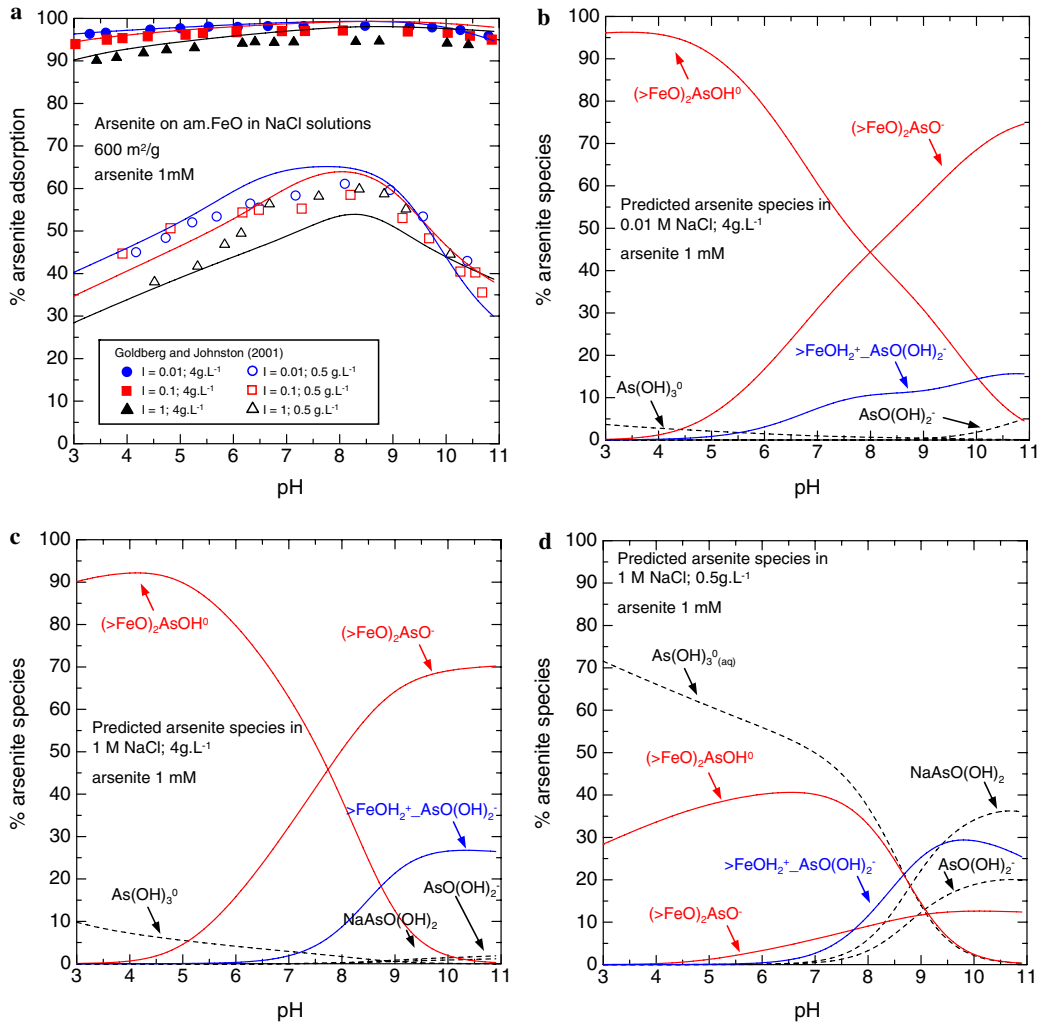

Fig. 7. As(III) adsorption on am.FeO. The curves were calculated with the ETLM using the arsenite surface species and parameters in Tables 1 and 2. (a) As(III) adsorption as a function of pH, ionic strength and surface coverage. The curves represent regression fits of the experimental data plotted as symbols. (b–d) Predicted model arsenite surface and aqueous speciation.

Goldberg and Johnston (2001). It is interesting that the experimental mobility data for am.AlO show significantly smaller shifts than observed for am.FeO (see above): 9.4 (no arsenic), 10.0 (with 0.01 mM As), and 9.3 (1 mM As). Under the same conditions, the isoelectric points are predicted to be 9.4, 9.4 and 8.7. The predicted values shift much less than in the case of am.FeO, which is in qualitative agreement with the experimental data. This arises because the deprotonated binuclear bidentate inner-sphere complex does not appear in the model.

The predicted model speciation of As(III) on the surface of am.AlO is given in Figs. 8b–d for the conditions $I = 0.01$ and 1.0 studied by Goldberg and Johnston (2001). It can be seen in the figures that the outer-sphere complex predominates from pH values of 7–10. The inner-sphere As(III) species is only important for am.AlO at pH values below about 5–6, depending on the ionic strength. In this regard, am.AlO behaves more like magnetite than am.FeO. The model speciation results shown in Figs. 8b–d are consistent with the dominance of outer-sphere As(III) on am.AlO inferred from FTIR studies by Goldberg and Johnston (2001).

3.8. Adsorption of As(III) on gibbsite from Weerasooriya et al. (2003)

The solid curves in Figs. 9a–c represent regression calculations using the inner- and outer-sphere species in Eqs. (1) and (3) and parameters in Tables 1 and 2. As in the case of goethite (Fig. 3), the data can be closely fit using only the inner-sphere As(III) species of Eq. (1). The outer-sphere species was included in the model solely to place an upper limit on its importance under the experimental conditions studied by Weerasooriya et al. (2003). Consequently, the value of $\log {}^{*}K^{0}_{\text{outer}}$ for gibbsite in Table 2 represents merely an upper limit. It can be seen in Figs. 9a–c that, with the exception of the lowest surface coverages at low pH at 0.01 M $NaNO_3$, the calculated curves provide a close description

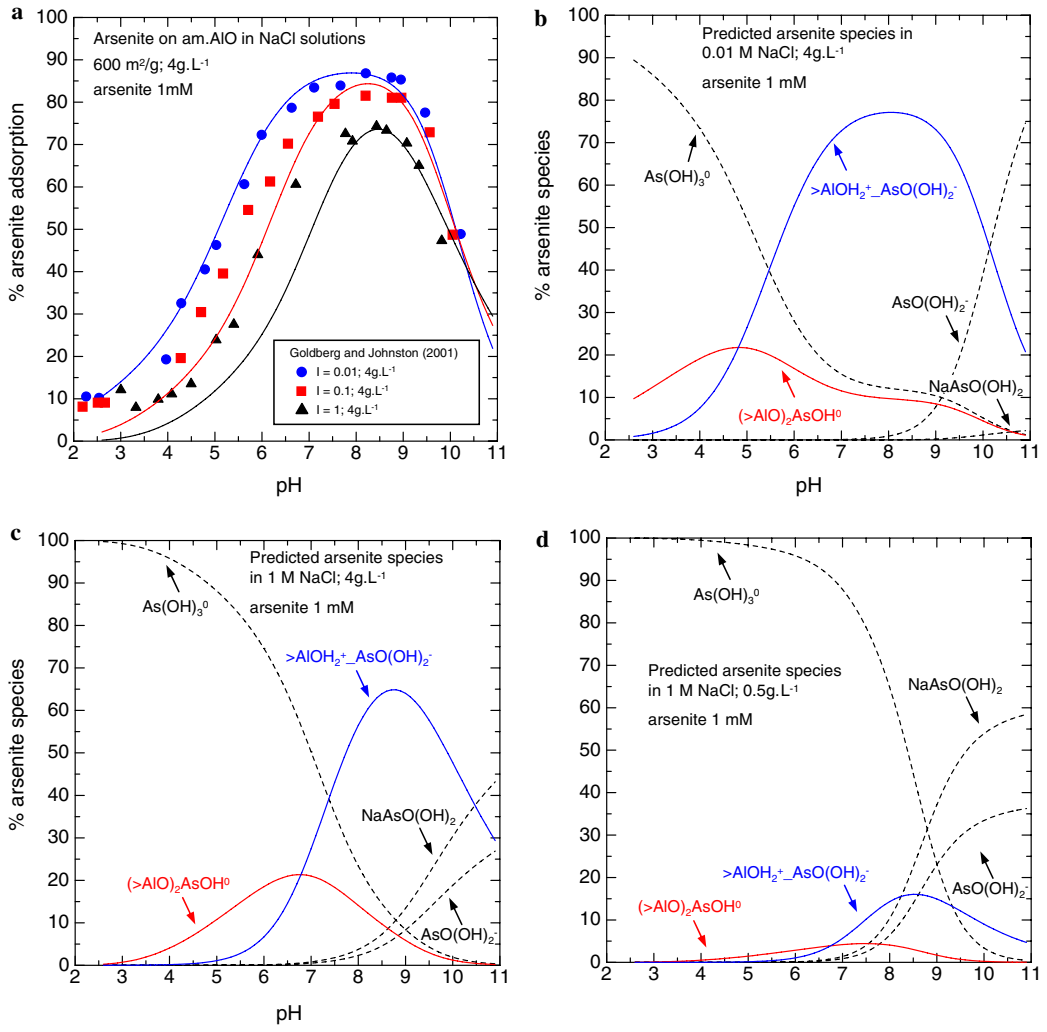

Fig. 8. As(III) adsorption on am.AlO. The curves were calculated with the ETLM using the arsenite surface species and parameters in Tables 1 and 2. (a) As(III) adsorption as a function of pH, ionic strength and surface coverage. The curves represent regression fits of the experimental data plotted as symbols. (b–d) Predicted model arsenite surface and aqueous speciation.

of the adsorption data over a wide range of pH and surface coverages in 0.001–0.1 M $NaNO_3$ solutions. The dominance of the inner-sphere species on gibbsite, α-$Al(OH)_3$, is consistent with the EXAFS and XANES results for As(III) on β-$Al(OH)_3$ from Arai et al. (2001). However, the current model differs dramatically from the CD-model presented by Weerasooriya et al. (2003) who inferred an outer-sphere complex was dominant based on the observed ionic strength dependence of adsorption, a small enthalpy of adsorption, and a small proton exchange ratio. The calculations reported in the present study are also consistent with small amounts of proton coadsorption (cf Fig. 6c).

The predicted model speciation of As(III) on the surface of gibbsite is given in Figs. 9d and e for the two surface coverages at $I = 0.001$ M studied by Weerasooriya et al. (2003). It can be seen here that the inner-sphere As(III) species is overwhelmingly dominant for gibbsite. This is a dramatic difference from the situation with am.AlO shown in Fig. 8.

4. Prediction of arsenite adsorption on all oxides

The regression calculations summarized above for magnetite, goethite, HFO, ferrihydrite, am.FeO, gibbsite, am.AlO and β-$Al(OH)_3$ have demonstrated that the reactions for protonated inner- and outer-sphere complexes given in Eqs. (1) and (3), i.e. $(>FeO)_2As(OH)^0$ and $>FeOH_2^+\_AsO(OH)_2^-$, can describe As(III) adsorption on these oxides under a very wide range of pH and ionic strengths, and a range of surface coverages from about $10^{-6.6}$ to $10^{-5.6}$ mol of As(III) m^{-2}. In contrast, the reactions producing the deprotonated inner-sphere and the additional outer-sphere complexes in Eqs. (5) and (7) have only been identified on ferrihydrite, am.FeO or HFO. Additional proton surface titration data in the presence of As(III) and much wider ranges of surface coverage are needed in order to investigate the possible importance of these species on other solids. Consequently, the remainder of this paper focusses on the two protonated species

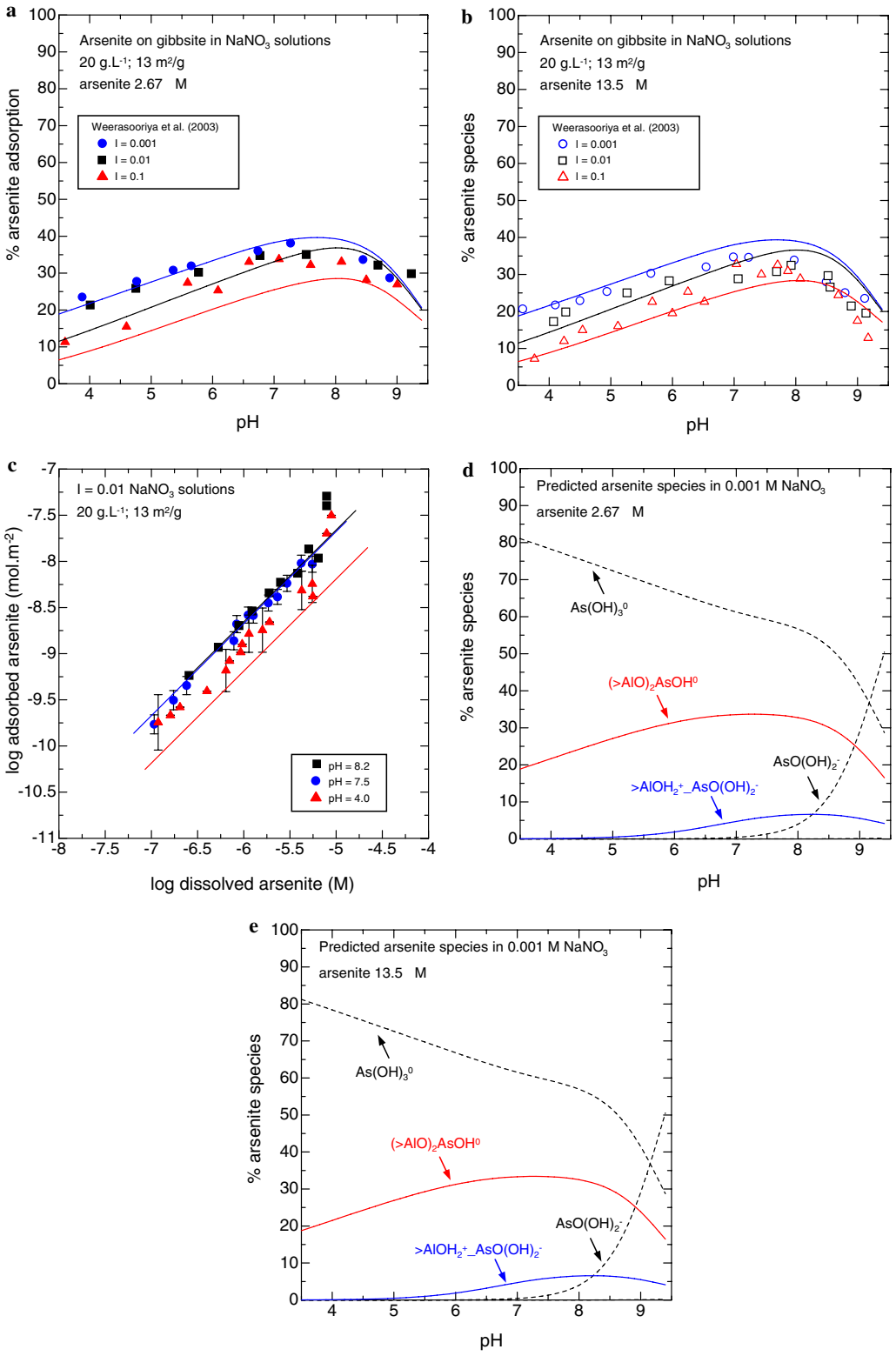

Fig. 9. As(III) adsorption on gibbsite. The curves were calculated with the ETLM using the arsenite surface species and parameters in Tables 1 and 2. (a–c) As(III) adsorption as a function of pH, ionic strength and surface coverage. The curves represent regression fits of the experimental data plotted as symbols. (d–e) Predicted model arsenite surface and aqueous speciation.

$(>FeO)_2As(OH)^0$ and $>FeOH_2^+\_AsO(OH)_2^-$ for which the most extensive results are recorded in Table 2. Which of these two species predominates, depends not only on the environmental parameters, but also on the nature of the solid (Figs. 2–9). In order to be able to unravel the dependence on the type of solid, the surface equilibrium constants for these species must be converted to an internally consistent set of site-occupancy standard states, as

well as corrected for differences in the pH_{ZPC} and ΔpK_n^θ of the solids. By so doing, systematic differences in the equilibrium constants from one solid to another can be investigated and explained on a theoretical basis. This permits prediction of As(III) adsorption equilibrium constants on all oxides, including those not yet studied experimentally.

The reactions forming the species $(>FeO)_2As(OH)^0$ and $>FeOH_2^+\_AsO(OH)_2^-$ used in the regression calculations in Figs. 2–9 have equilibrium constants $\log {}^*K^0_{(>SO)_2As(OH)^0}$ and $\log {}^*K^0_{>SOH_2^+\_AsO(OH)_2^-}$, respectively, given in Table 2. Conversion of these equilibrium constants to site-occupancy standard states, as well as correcting for differences in the pH_{ZPC} and ΔpK_n^θ of the solids, can be made with the following equations:

$$\log K^\theta_{(>SO)_2As(OH)^0} = \log {}^*K^0_{(>SO)_2As(OH)^0} - 2pH_{ZPC} + \Delta pK_n^\theta + \log\left(\frac{(N_sA_s)^2}{N^\ddagger A^\ddagger}C_s\right) \quad (22)$$

$$\log K^\theta_{>SOH_2^+\_AsO(OH)_2^-} = \log {}^*K^0_{outer} - pH_{ZPC} + \frac{\Delta pK_n^\theta}{2} + \log\left(\frac{N_sA_s}{N^\ddagger A^\ddagger}\right) \quad (23)$$

where $\log K^\theta_{(>SO)_2As(OH)^0}$ and $\log K^\theta_{>SOH_2^+\_AsO(OH)_2^-}$ refer to site-occupancy standard states and the reactions

$$2\,>SOH_2^+ + As(OH)_3^0 = (>SO)_2As(OH)^0 + 2H^+ + 2H_2O \quad (24)$$

and

$$>SOH_2^+ + As(OH)_3^0 = >SOH_2^+\_AsO(OH)_2^- + H^+ \quad (25)$$

The values of $\log K^\theta_{(>SO)_2As(OH)^0}$ and $\log K^\theta_{>SOH_2^+\_AsO(OH)_2^-}$ listed in Table 2 were calculated with Eqs. (22) and (23) and the parameters in Table 1. Overall uncertainties in the final equilibrium constants are difficult to assess because they will include uncertainties from regression of the experimental data (about ±0.2 in $\log K$ values) as well as uncertainties from the parameters in Eqs. (22) and (23) such as estimated values of the pH_{ZPC}. Overall, it is estimated that the uncertainties in the $\log K$ values in Table 2 may be ±0.5 units.

Eqs. (24) and (25) differ because of the explicit release of two moles of water molecules during the formation of the inner-sphere complex (see also Fig. 1). As shown above, this release strongly affects the electrostatic energy of the reaction. In a first approximation, we distinguish the release of this water from the release of waters of solvation associated with the adsorbing ions, which will occur strongly for the inner-sphere complex and to a lesser extent for the outer-sphere complex. Solvation waters are not explicitly shown in either Eqs. (24) or (25). Nevertheless, the free energy of this solvation process plays a critical role in the overall adsorption process. In previous theoretical studies of proton, electrolyte cation and anion, and divalent metal ion adsorption (James and Healy, 1972; Sverjensky, 1993; Sverjensky and Sahai, 1996; Sahai and Sverjensky, 1997; Sverjensky, 2005; Sverjensky, 2006), it has been discovered that the solvation free energy associated with an adsorbing ion can be a major determinant of the differences in the overall equilibrium constants for different solids. The solvation free energy associated with the removal of water molecules from an adsorbing ion opposes the adsorption process. Born solvation theory predicts that the magnitude of the opposition varies from one solid to another, thereby enabling explanation of the differences in equilibrium constants for adsorption of a given ion on a variety of solids.

In the present study, we assume that the overall equilibrium constant for adsorption forming the jth As(III) surface species ($\log K_j^\theta$), referring to either Eqs. (24) or (25), can be expressed in terms of a solvation contribution and an intrinsic binding contribution (Sverjensky, 2005, 2006) such that

$$\log K_j^\theta = \frac{-\Delta\Omega_{r,j}}{2.303RT}\left(\frac{1}{\varepsilon_s}\right) + \log K''_{ii,j} \quad (26)$$

In Eq. (26), the first term on the right-hand side is derived from Born solvation theory. It contains $\Delta\Omega_{r,j}$, which represents a Born solvation coefficient for the reaction forming the jth species, and ε_s, which represents the dielectric constant of the sth solid. The second term, $\log K''_{ii,j}$, represents an intrinsic binding of arsenite independent of the type of oxide, but also includes terms derived from solvation theory dependent on the dielectric constant of the interfacial water. It is assumed here that $\log K''_{ii,j}$ is a constant for a given reaction. The values of ε_s used in the present study are summarised in Table 2. As already noted above, those for the HFO, ferrihydrite, am.FeO and am.AlO of the present study were obtained by estimation from the pH_{ZPC}, using equations based on Born solvation and crystal chemical theory in Sverjensky (2005). The utility of these estimated dielectric constants is tested by using them in the regression of the $\log K_j^\theta$ values for As species with Eq. (26).

Regression of values of $\log K^\theta_{(>SO)_2As(OH)^0}$ and $\log K^\theta_{>SOH_2^+\_AsO(OH)_2^-}$ from Table 2 with Eq. (26) using dielectric constants from Table 2 resulted in the lines of best fit shown in Figs. 10a and b and the equations

$$\log K^\theta_{(>SO)_2As(OH)^0} = -54.36\left(\frac{1}{\varepsilon_s}\right) + 1.83 \quad (27)$$

$$\log K^\theta_{>SOH_2^+\_AsO(OH)_2^-} = -38.23\left(\frac{1}{\varepsilon_s}\right) + 0.69 \quad (28)$$

It can be seen in Fig. 10 that most of the datapoints used in the regression agree with the calculated lines within the uncertainties depicted (±0.5). This indicates that the simple solvation theory expressed in Eq. (26) can account quantitatively for the experimentally derived differences in As(III) $\log K$ values. Even where the dielectric constants of amorphous or poorly crystalline solids have been estimated from values of the pH_{ZPC}, e.g. for HFO, ferrihydrite, am.FeO and am.AlO, six out of the eight corresponding points plotted in Fig. 10 are remarkably close to the data derived for the crystalline oxides. This establishes that the large differences in the equilibrium constants for adsorption of As(III)

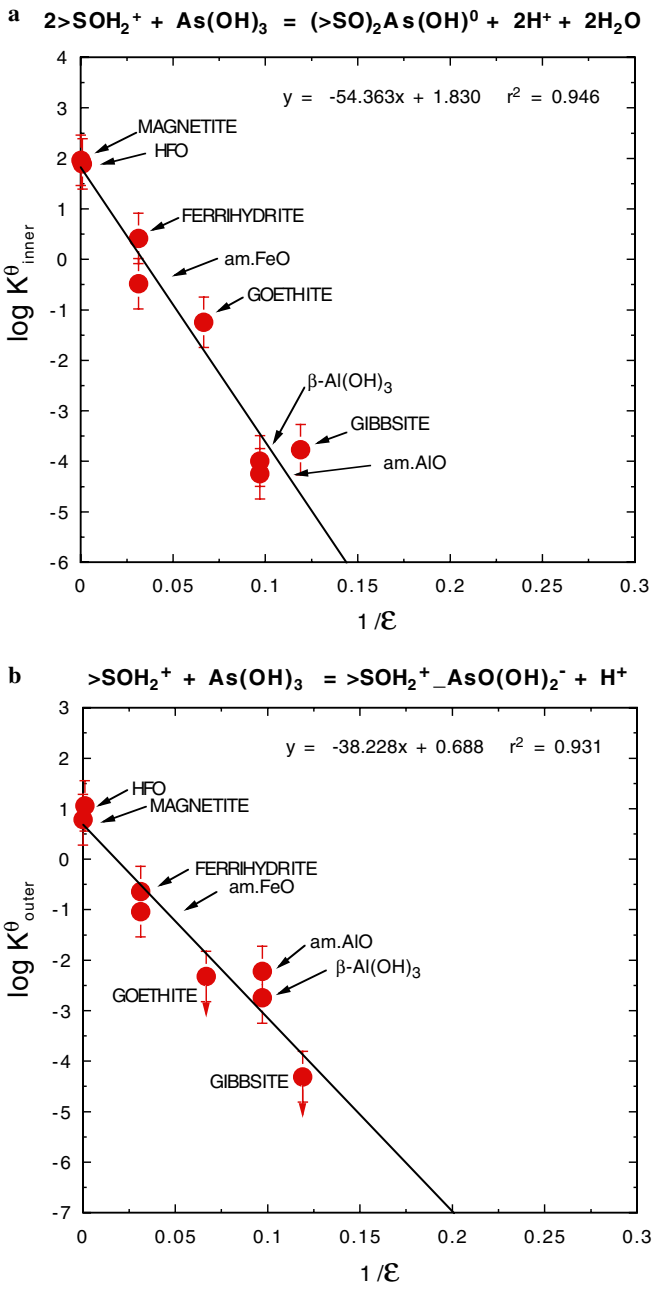

Fig. 10. Correlation of the logarithms of the equilibrium constants for inner- and outer-sphere As(III) adsorption on oxides with the inverse of the dielectric constant of the oxide (Table 3). The lines were generated by regression with Eqs. (27) and (28). The equilibrium constants were obtained by analysis of the data in Figs. 2–9, are consistent with site-occupancy standard states, and were corrected for differences in the pH_{ZPC} and ΔpK_n^θ of the oxides. The error bars represent uncertainties of ±0.5 in the $\log K$ values. The arrows for goethite and gibbsite in (b) indicate that these values are upper limits only.

on amorphous and poorly crystalline oxides of different kinds can be accounted for with Born solvation theory. In other words, there appear to be significant differences in the surface chemistry of these oxides. Additional experimental studies are required to investigate this issue.

It can also be seen in Fig. 10a that the slope for the inner-sphere reaction is significantly larger than that for the outer-sphere reaction in Fig. 10b, indicating that the solvation effect, i.e. the extent of dehydration of the adsorbing ion, is much stronger for the formation of the inner- than the outer-sphere species, as would be expected. Similarly, the magnitude of the intercept term in Eq. (27) is greater than two times the intercept in Eq. (28). This term is related to the intrinsic binding of As(III) that would be expected to be stronger for an inner-sphere species. The fact that a bulk property of the solid, the dielectric constant, provides a theoretical explanation of systematic differences in As(III) surface equilibrium constants from one solid to another strongly suggests that Eqs. (27) and (28) can be used to predict the values of $\log K^\theta_{(>SO)_2As(OH)^0}$ and $\log K^\theta_{>SOH_2^+\_AsO(OH)_2^-}$ for other solids. The results of such predictions are given in Table 3. Uncertainties in the predicted values of $\log K^\theta_{(>SO)_2As(OH)^0}$ and $\log K^\theta_{>SOH_2^+\_AsO(OH)_2^-}$ are at least ±0.5 based on the correlations in Fig. 10. However, additional uncertainties are associated with the use of the predicted equilibrium constants.

In practise, computer codes calculating surface reactions will often require values of $\log {}^*K^0_{(>SO)_2As(OH)^0}$ and $\log {}^*K^0_{>SOH_2^+\_AsO(OH)_2^-}$, which refer to the hypothetical 1.0 M standard state and the reactions in Eqs. (1) and (3) above, rather than those in Eqs. (24) and (25). Values of $\log {}^*K^0_{(>SO)_2As(OH)^0}$ and $\log {}^*K^0_{>SOH_2^+\_AsO(OH)_2^-}$ can be calculated with the equations

Table 3
Predicted equilibrium constants for As(III) adsorption on oxides consistent with the extended triple-layer model:[a]

$\log K^\theta_{(>SO)_2As(OH)^0}: 2>SO^- + 2H^+ + As(OH)_3^0 = (>SO)_2As(OH)^0 + 2H_2O$

$\log K^\theta_{>SOH_2^+\_AsO(OH)_2^-}: >SO^- + H^+ + As(OH)_3^0 => SOH_2^+\_AsO(OH)_2^-$

Solid	ε_s[b]	$\log K^\theta_{(>SO)_2As(OH)^0}$	$\log K^\theta_{>SOH_2^+\_AsO(OH)_2^-}$
Fe_3O_4	1000	1.8	0.7
HFO	1000[c]	1.8	0.7
α-MnO_2	1000	1.8	0.7
α-TiO_2	121	1.4	0.4
Ferrihydrite	32[c]	0.1	−0.5
am.FeO	32[c]	0.1	−0.5
β-TiO_2	18.6	−1.1	−1.4
FeOOH	15	−1.8	−1.9
Fe_2O_3	12	−2.7	−2.5
α-Al_2O_3	10.4	−3.4	−3.0
γ-Al_2O_3	10.4	−3.4	−3.0
am.AlO	10.3[c]	−3.4	−3.0
β-$Al(OH)_3$	10.3[c]	−3.4	−3.0
α-$Al(OH)_3$	8.4	−4.6	−3.9
α-SiO_2	4.6	−10.0	−7.7
am.SiO_2	3.8	−12.4	−9.4

[a] Calculated with Eqs. (27) and (28) and the dielectric constants tabulated.

[b] Dielectric constant of the solid from Sverjensky (2005) unless otherwise noted.

[c] Values estimated with the aid of the theoretical equation relating pH_{ZPC} and $\frac{1}{\varepsilon_s}$ (Sverjensky, 2005) using values of the pH_{ZPC} equal to 7.9 (HFO), 8.5 (ferrihydrite and am.FeO), 9.4 (am.AlO), and 9.3 (β-$Al(OH)_3$).

$$\log {}^{*}K^{0}_{(>SO)_2As(OH)^0} = \log K^{\theta}_{(>SO)_2As(OH)^0} + 2pH_{ZPC} - \Delta pK^{\theta}_{n} - \log\left(\frac{(N_sA_s)^2}{N^{\ddagger}A^{\ddagger}}C_s\right) \quad (29)$$

$$\log {}^{*}K^{0}_{outer} = \log K^{\theta}_{outer} + pH_{ZPC} - \frac{\Delta pK^{\theta}_{n}}{2} - \log\left(\frac{N_sA_s}{N^{\ddagger}A^{\ddagger}}\right) \quad (30)$$

It can be seen in Eqs. (29) and (30) that predicted values of $\log {}^{*}K^{0}_{(>SO)_2As(OH)^0}$ and $\log {}^{*}K^{0}_{>SOH^{+}_{2}\_AsO(OH)^{-}_{2}}$ will be sensitive to the values of pH_{ZPC}, ΔpK^{θ}_{n}, the site density and the surface area of the solids. This will produce additional uncertainties in the predictions. The values of pH_{ZPC} to be used in Eqs. (29) and (30), as well as in Eqs. (22) and (23), should be chosen carefully. Values of the point-of-zero-salt effect (pH_{PZSE}) should not be used without correction because such values are generally dependent on the type of electrolyte and can differ from a pristine-point-of-zero charge by as much as 0.2 to 0.5 (Sverjensky, 2005). Ideally, an experimentally determined isoelectric point (IEP) referring to low ionic strengths ($I \leqslant 0.01$) should be used. However, in the absence of an experimental IEP, the pH_{ZPC} can be estimated from an experimental pH_{PZSE} using the equation

$$pH_{PZC} = pH_{PZSE} - 0.5(\log K^{\theta}_{L^-} - \log K^{\theta}_{M^+}) \quad (31)$$

together with predicted values of $\log K^{\theta}_{M^+}$ and $\log K^{\theta}_{L^-}$ for the background electrolyte ML (Sverjensky, 2005). Eq. (31) corrects values of the pH_{PZSE} determined from the intersection of proton titration curves referring to different ionic strengths to generate pH_{ZPC} independent of electrolyte effects.

5. Concluding remarks

The regression calculations and correlations discussed above strongly support application of the dipole modification of the triple-layer model, the ETLM, to establishing the surface speciation of adsorbed As(III) under a wide range of conditions on oxides in simple electrolyte solutions. The results of the present study permit the following observations about As(III) surface speciation:

(1) Two principal reactions forming inner- and outer-sphere As(III) surface species,

$$2\,{>}SOH + As(OH)^0_3 = (>SO)_2As(OH)^0 + 2H_2O$$

and

$$>SOH + As(OH)^0_3 = >SOH^{+}_{2}\_AsO(OH)^{-}_{2},$$

respectively, were found to be consistent with adsorption experiments referring to wide ranges of pH, ionic strength, an order of magnitude in surface coverage and a variety of types of solids reported in the literature (Wilkie and Hering, 1996; Jain et al., 1999a; Jain and Loeppert, 2000; Goldberg and Johnston, 2001; Weerasooriya et al., 2003; Dixit and Hering, 2003). Under some circumstances, an additional inner- and an additional outer-sphere complex were needed to describe the data. On ferrihydrite and am.FeO the additional inner-sphere species is also bidentate–binuclear, but is deprotonated. It is represented by

$$2\,{>}SOH + As(OH)^0_3 = (>SO)_2AsO^- + H^+ + 2H_2O$$

On HFO, at very low surface coverages, about $10^{-6.6}$ to $10^{-7.4}$ mol of As(III) m^{-2}, the additional outer-sphere species is represented by

$$2\,{>}SOH + H^+ + As(OH)^0_3 = (>SOH^{+}_{2})_2\_AsO(OH)^{-}_{2}$$

The existence of inner-sphere, bidentate, binuclear and outer-sphere surface species is consistent with all EXAFS and XANES studies (Manning et al., 1998; Arai et al., 2001; Farquhar et al., 2002). The present calculations indicate that any outer-sphere As(III) species on goethite would be present at concentrations less than about 10% of the inner-sphere concentrations. Under some circumstances, this may be too low to be detected by XAFS.

(2) Possible protonation states of the two main surface As(III) species were established in the present study by surface complexation modelling. Definitive spectroscopic results for comparison with the model species are not available. FTIR studies of As(III) have suggested the existence of a doubly protonated surface species on am.FeO (Suarez et al., 1998), but have not yet identified if there is more than one surface species present. Gas-phase DFT calculations have suggested a bidentate–binuclear species which could be represented as $(>FeO)_2As(OH)^0$. The protonation states of this species is the same as that established in the present study. The protonation states proposed in the present study for the two main As(III) species are also consistent with two more indirect lines of experimental evidence. First, measured As/H release data are consistent with the above two reactions. Second, model predictions of the zeta potential for alumina and am. AlO in arsenite solutions (assuming $\zeta = \psi_d$) show small displacements of the isoelectric point, consistent with extrapolation of trends in electrophoretic mobility data with pH (Arai et al., 2001; Goldberg and Johnston, 2001). The larger shifts in the isoelectric point measured for am.FeO (Goldberg and Johnston, 2001) are explained in the present study by the possible existence of the deprotonated species indicated above.

(3) The equilibrium constants $\log {}^{*}K^{0}_{(>SO)_2As(OH)^0}$ and $\log {}^{*}K^{0}_{>SOH^{+}_{2}\_AsO(OH)^{-}_{2}}$ referring to the hypothetical 1.0 M standard state and the pH_{ZPC} and ΔpK^{θ}_{n} of the specific solids have been converted to an internally consistent set of site-occupancy standard states. The resultant values of $\log K^{\theta}_{(>SO)_2As(OH)^0}$ and $\log K^{\theta}_{>SOH^{+}_{2}\_AsO(OH)^{-}_{2}}$ are independent of the specific

surface areas, site densities, solid concentrations as well as the pH_{ZPC} and ΔpK_n^θ of the solids used in the original experiments. The values of $\log K^\theta_{(>SO)_2As(OH)^0}$ and $\log K^\theta_{>SOH_2^+\_AsO(OH)_2^-}$ are also consistent with a set of surface protonation and electrolyte adsorption equilibrium constants which themselves are consistent with site-occupancy standard states independent of the specific surface areas and site densities of the solids. These internal consistencies throughout the model are essential in order to sensibly compare the As(III) equilibrium constants for different solids, or different samples of the same solid, and to place As(III) adsorption on a predictive basis.

(4) Systematic differences in the values of $\log K^\theta_{(>SO)_2As(OH)^0}$ and $\log K^\theta_{>SOH_2^+\_AsO(OH)_2^-}$ have been established for As(III) adsorption on different solids. These differences can be explained by the application of Born solvation theory. The solvation free energy associated with As(III) adsorbing to a variety of solids is a major determinant of the differences in the overall equilibrium constants. It arises from the work required to remove water molecules from the adsorbing As(III), which opposes the adsorption process.

(5) Regression of the values of $\log K^\theta_{(>SO)_2As(OH)^0}$ and $\log K^\theta_{>SOH_2^+\_AsO(OH)_2^-}$ based on Born solvation theory has resulted in a set of predictive equations for As(III) adsorption equilibrium constants on all oxides. All that is needed to make predictions is a value of the dielectric constant of the solid. Where experimental values of this quantity are not available, e.g. for a variety of amorphous iron or aluminum oxides, effective dielectric constants have been estimated using values of the pH_{ZPC} and theoretical equations previously developed (Sverjensky, 2005). This enables consideration of both amorphous and crystalline oxides within the predictive framework. Predicted values of $\log K^\theta_{(>SO)_2As(OH)^0}$ and $\log K^\theta_{>SOH_2^+\_AsO(OH)_2^-}$ can be converted to equilibrium constants specific to solid samples with known surface areas, site densities, and pH_{ZPC} values.

The results summarized above establish a predictive surface complexation model useful for calculating the conditions under which different surface species of As(III) may be important on a wide range of oxides in simple electrolyte solutions. This is a first step in assessing the role of adsorption in the environmental geochemistry of arsenic. Combination of the present results with a similar study for As(V) will permit the competitive adsorption of As(III) and (V) to be investigated for comparison with experimental results (Goldberg, 2002). A competitive adsorption model for As(III) and (V) will enable assessment of the role of oxide surfaces in stabilizing one oxidation state relative to the other. Similarly, it will be necessary to investigate the role of competitive adsorption by other anions such as sulfate (Wilkie and Hering, 1996), carbonate, silicate, and organic species. All of these features can be progressively added to the ETLM in order to establish a more comprehensive quantitative approach to understanding the geochemistry of arsenic in natural systems.

Acknowledgments

We greatly appreciate discussions with Y. Arai, J.A. Davis, D.B. Kent, and G.A. Waychunas. We also wish to thank J. Kubicki and P. O'Day for reading the manuscript and making useful suggestions. D.A. Sverjensky thanks the Geophysical Laboratory of the Carnegie Institute of Washington and Bob Hazen for hosting him during the preparation of this manuscript. Financial support was provided by DuPont Engineering and DOE Grant DE-FG02-96ER-14616.

Associate editor: Peggy A. O'Day

Appendix A. Standard states used in the present study

Equilibrium constants in the present study, K^θ, refer to site-occupancy standard states denoted by the superscript "θ" (Sverjensky, 2003). The standard state for sorbent sites (>SOH) refers to unit activity of surface sorption sites on a completely unsaturated surface at any P and T such that

$$a_{>SOH} = \lambda_{>SOH} X_{>SOH} \tag{A.1}$$

and $\lambda_{>SOH} \to 1$ as $X_{>SOH} \to 1$. In Eq. (A.1), $a_{>SOH}$, $\lambda_{>SOH}$ and $X_{>SOH}$ represent the activity, activity coefficient and mole fraction of >SOH sites, respectively. For sorbate species ($>j$), the standard state refers to unit activity of surface species on a completely saturated surface with zero potential at any P and T referenced to infinite dilution, expressed by

$$a_{>j} = \lambda_{>j} X_{>j} \tag{A.2}$$

where $\lambda_{>j} \to 1$ and the potential ψ associated with $>j$ approach zero as $X_{>j} \to 0$. In Eq. (A.2), $a_{>j}$, $\lambda_{>j}$ and $X_{>j}$ represent the activity, activity coefficient and mole fraction of the $>j$th sorbate species, respectively. In TLM calculations, the limiting conditions of $X_{>SOH} \to 1$ and $X_{>j} \to 0$ are often approached. In other words, >SOH is commonly by far the dominant species, whereas sorbates are minor species. Under these circumstances, it is reasonable to assume that $\lambda_{>SOH} \approx 1$ and $\lambda_{>j} \approx 1$.

The site-occupancy standard states are related to the widely used hypothetical 1.0 M standard state (Sverjensky, 2003) by

$$\log K_1^\theta = \log K_1^0 + \log\left(\frac{N_s A_s}{N^\ddagger A^\ddagger}\right) \tag{A.3}$$

$$\log K_2^\theta = \log K_2^0 - \log\left(\frac{N_s A_s}{N^\ddagger A^\ddagger}\right) \tag{A.4}$$

$$\log K_{ZPC}^\theta = \log K_{ZPC}^0 = 2pH_{ZPC} \tag{A.5}$$

and

$$\Delta pK_n^\theta = \log K_n^\theta = \log K_n^0 - 2\left(\frac{N_s A_s}{N^\ddagger A^\ddagger}\right) \quad (A.6)$$

where the superscript "0" represents the hypothetical 1.0 M standard state and N_s represents the surface site density on the sth solid sorbent (sites m^{-2}); $N^\ddagger$ represents the standard state sorbate species site density (sites m^{-2}); A_s represents the BET surface area of the sth solid sorbent ($m^2\ g^{-1}$); $A^\ddagger$ represents a standard state BET surface area ($m^2\ g^{-1}$).

In the present study, values of $N^\ddagger = 10 \times 10^{18}$sites m^{-2} and $A^\ddagger = 10\ m^2\ g^{-1}$ are selected for all solids. It is emphasized that these values are properties of the hypothetical standard state applicable to all samples of all solids.

Equilibria for adsorption of the monovalent electrolyte ions M^+ and L^- can be expressed by

$$>SOH + M^+ = >SO^-\_M^+ + H^+ \quad (A.7)$$

and

$$>SOH + H^+ + L^- = >SOH_2^+\_L^- \quad (A.8)$$

for which

$$\log {}^*K_{M^+}^\theta = \log {}^*K_{M^+}^0 + \log\left(\frac{N_s A_s}{N^\ddagger A^\ddagger}\right) \quad (A.9)$$

and

$$\log {}^*K_{L^-}^\theta = \log {}^*K_{L^-}^0 + \log\left(\frac{N_s A_s}{N^\ddagger A^\ddagger}\right) \quad (A.10)$$

When the electrolyte adsorption reactions are written relative to the charged surface species $>SOH_2^+$ and $>SO^-$,

$$>SO^- + M^+ = >SO^-\_M^+ \quad (A.11)$$

and

$$>SOH_2^+ + L^- = >SOH_2^+\_L^- \quad (A.12)$$

it follows that

$$\log K_{M^+}^\theta = \log {}^*K_{M^+}^\theta + \log K_2^\theta = \log {}^*K_{M^+}^0 + \log K_2^\theta + \log\left(\frac{N_s A_s}{N^\ddagger A^\ddagger}\right) \quad (A.13)$$

and

$$\log K_{L^-}^\theta = \log {}^*K_{L^-}^\theta - \log K_1^\theta = \log {}^*K_{L^-}^0 - \log K_1^\theta + \log\left(\frac{N_s A_s}{N^\ddagger A^\ddagger}\right) \quad (A.14)$$

where the absence of the superscript "*" denotes the reaction written (as above) relative to $>SOH_2^+$ and $>SO^-$.

In practice, theoretically predicted values of $\log K_{M^+}^\theta$ and $\log K_{L^-}^\theta$ must often be converted to values of $\log {}^*K_{M^+}^0$ and $\log {}^*K_{L^-}^0$ for use in computer codes referring to the hypothetical 1.0 M standard state and >SOH reactant species. This can conveniently be done using the following equations:

$$\log {}^*K_{M^+}^0 = \log K_{M^+}^\theta - pH_{ZPC} - \Delta pK_n^\theta - \log\left(\frac{N_s A_s}{N^\ddagger A^\ddagger}\right) \quad (A.15)$$

and

$$\log {}^*K_{L^-}^0 = \log K_{L^-}^\theta + pH_{ZPC} - \Delta pK_n^\theta - \log\left(\frac{N_s A_s}{N^\ddagger A^\ddagger}\right) \quad (A.16)$$

In the present study, equilibria for adsorption of As(III) expressed as the arsenite ion are given by

$$2\ >SOH + As(OH)_3^0 = (>SO)_2As(OH)^0 + 2H_2O \quad (A.17)$$

where

$${}^*K_{(>SO)_2As(OH)^0}^\theta = \frac{a_{(>SO)_2As(OH)^0} a_{H_2O}^2}{a_{>SOH}^2 a_{As(OH)_3^0}} 10^{\frac{F(0)}{2.303RT}} \quad (A.18)$$

and

$$>SOH + As(OH)_3^0 = >SOH_2^+\_AsO(OH)_2^- \quad (A.19)$$

where

$${}^*K_{outer}^\theta = \frac{a_{>SOH_2^+\_AsO(OH)_2^-}}{a_{>SOH} a_{As(OH)_3^0}} 10^{\frac{F(\psi_0 - \psi_\beta)}{2.303RT}} \quad (A.20)$$

The relationship to the hypothetical 1.0 M standard state is given by

$$\log {}^*K_{(>SO)_2As(OH)^0}^\theta = \log {}^*K_{(>SO)_2As(OH)^0}^0 + \log\left(\frac{(N_s A_s)^2}{N^\ddagger A^\ddagger} C_s\right) \quad (A.21)$$

$$\log {}^*K_{outer}^\theta = \log {}^*K_{outer}^0 + \log\left(\frac{N_s A_s}{N^\ddagger A^\ddagger}\right) \quad (A.22)$$

Using these equations, values of ${}^*K_{(>SO)_2As(OH)^0}^0$ and ${}^*K_{outer}^0$ are converted to ${}^*K_{(>SO)_2As(OH)^0}^\theta$ and ${}^*K_{outer}^\theta$ referring to site-occupancy standard states. The resultant values of ${}^*K_{(>SO)_2As(OH)^0}^\theta$ and ${}^*K_{outer}^\theta$ are independent of the site density, surface area or solid concentration of the specific samples used in the experiments. The utility of this conversion can be seen in the correlation graphs in Fig. 10 of the text.

References

Arai, Y., Elzinga, E., Sparks, D.L., 2001. X-ray absorption spectroscopic investigation of arsenite and arsenate adsorption at the aluminum oxide–water interface. *J. Colloid Interface Sci.* **235**, 80–88.

Arai, Y., Sparks, D.L., Davis, J.A., 2004. Effects of dissolved carbonate on arsenate adsorption and surface speciation at the hematite–water interface. *Environ. Sci. Technol.* **38**, 817–824.

Blesa, M.A., Weisz, A.D., Morando, P.J., Salfity, J.A., Magaz, G.E., Regazzoni, A.e., 2000. The interaction of metal oxide surfaces with complexing agents dissolved in water. *Coordin. Chem. Rev.* **196**, 31–63.

Bockris, J.O.M., Reddy, A.K.N., 1970. Modern Electrochemistry. Plenum Press.

Criscenti, L.J., Sverjensky, D.A., 1999. The role of electrolyte anions ClO_4^-, NO_3^-, and Cl^- in divalent metal (M^{2+}) adsorption on oxide and hydroxide surfaces in salt solutions. *Am. J. Sci.* **299**, 828–899.

Criscenti, L.J., Sverjensky, D.A., 2002. A single-site model for divalent and heavy metal adsorption over a range of metal concentrations. *J. Colloid Interface Sci.* **253**, 329–352.

Davis, J.A., Kent, D.B., 1990. Surface complexation modeling in aqueous geochemistry. In: Hochella, Jr., M.F., White, A.F. (Eds.), *Mineral–Water Interface Geochemistry*, Vol. 23. Mineralogical Society of America, pp. 177–259.

Davis, J.A., Leckie, J.O., 1978. Surface ionization and complexation at the oxide/water interface II. Surface properties of amorphous iron oxyhydroxide and adsorption of metal ions. *J. Colloid Interface Sci.* **67**, 90–107.

Davis, J.A., Leckie, J.O., 1980. Surface ionization and complexation at the oxide/water interface 3. Adsorption of anions. *J. Colloid Interface Sci.* **74**, 32–43.

Dixit, S., Hering, J.G., 2003. Comparison of arsenic(V) and arsenic (III) sorption onto iron oxide minerals: Implications for arsenic mobility. *Environ. Sci. Technol.* **37**, 4182–4189.

Farquhar, M.L., Charnock, J.M., Livens, F.R., Vaughan, D.J., 2002. Mechanisms of arsenic uptake fom aqueous solution by interaction with goethite, lepidocrocite, mackinawite, and pyrite: an X-ray absorption spectroscopy study. *Environ. Sci. Technol.* **36**, 1757–1762.

Filius, J.D., Hiemstra, T., van Riemsdijk, W.H., 1997. Adsorption of small weak organic acids on goethite: modelling of mechanisms. *J. Colloid Interface Sci.* **195**, 368–380.

Geelhoed, J.S., Hiemstra, T., van Riemsdijk, W.H., 1997. Phosphate and sulfate adsorption on goethite: Single anion and competitive adsorption. *Geochim. Cosmochim. Acta* **61**, 2389–2396.

Goldberg, S., 2002. Competitive adsorption of arsenate and arsenite on oxides and clay minerals. *Soil Sci. Am. J.* **66**, 413–421.

Goldberg, S., Johnston, C.T., 2001. Mechanisms of arsenic adsorption on amorphous oxides evaluated using macroscopic measurements, vibrational spectroscopy, and surface complexation modeling. *J. Colloid Interface Sci.* **234**, 204–216.

Grafe, M., Eick, M.J., Grossl, P.R., 2001. Adsorption of arsenate (V) and arsenite (III) on goethite in the presence and absence of dissolved organic carbon. *Soil Sci. Am. J.* **65**, 1680–1687.

Grafe, M., Eick, M.J., Grossl, P.R., Saunders, A.M., 2002. Adsorption of arsenate (V) and arsenite (III) on ferrihydrite in the presence and absence of dissolved organic carbon. *J. Environ. Qual.* **31**, 1115–1123.

Grossl, P., Eick, M.J., Sparks, D.L., Goldberg, S., Ainsworth, C.C., 1997. Arsenate and chromate retention mechanisms on goethite. 2. Kinetic evaluation using a pressure-jump relaxation technique. *Environ. Sci. Technol.* **31**, 321–326.

Helgeson, H.C., Kirkham, D.H., Flowers, G.C., 1981. Theoretical prediction of the thermodynamic behavior of aqueous electrolytes at high pressures and temperatures. IV. Calculation of activity coefficients, osmotic coefficients, and apparent molal and standard and relative partial molal properties to 5 kb and 600 ^{0}C. *Am. J. Sci.* **281**, 1241–1516.

Hiemstra, T., van Riemsdijk, W.H., 1996. A surface structural approach to ion adsorption: the charge distribution (CD) model. *J. Colloid Interface Sci.* **179**, 488–508.

Hiemstra, T., van Riemsdijk, W.H., 1999. Surface structural ion adsorption modeling of competitive binding of oxyanions by metal (hydr)oxides. *J. Colloid Interface Sci.* **210**, 182–193.

Hiemstra, T., van Riemsdijk, W.H., 2000. Fluoride adsorption on goethite in relation to different types of surface sites. *J. Colloid Interface Sci.* **225**, 94–104.

Hug, S.J., 1997. In situ Fourier transform infrared measurements of sulfate adsorption on hematite in aqueous solutions. *J. Colloid Interface Sci.* **188**, 415–422.

Jain, A., Loeppert, R.H., 2000. Effect of competing anions on the adsorption of arsenite and arsenate by ferrihydrite. *J. Environ. Qual.* **29**, 1423–1430.

Jain, A., Raven, K.P., Loeppert, R.H., 1999a. Arsenite and arsenate adsorption on ferrihydrite: surface charge reduction and OH- release stoichiometry. *Environ. Sci. Technol.* **33**, 1179–1184.

Jain, A., Raven, K.P., Loeppert, R.H., 1999b. Response to comment on "Arsenite and arsenate adsorption on ferrihydrite: surface charge reduction and OH- release stoichiometry". *Environ. Sci. Technol.* **33**, 3696.

James, R.O., Healy, T.W., 1972. Adsorption of hydrolyzable metal ions at the oxide–water interface III. A thermodynamic model of adsorption. *J. Colloid Interface Sci.* **40**, 65–81.

Kubicki, J.D., 2005. Comparison of As(III) and As(V) complexation onto Al- and Fe-hydroxides. In: Benning, L. (Ed.), *Advances in Arsenic Research: Integration of Experimental and Observational Studies and Implications for Migration*, vol. 915. American Chemical Society, pp. 104–117.

Manning, B.A., Fendorf, M., Goldberg, S., 1998. Surface structures and stability of arsenic(III) on goethite: spectroscopic evidence for inner-sphere complexes. *Environ. Sci. Technol.* **32**, 2383–2388.

Manning, B.A., Goldberg, S., 1997. Adsorption and stability of arsenic(III) at the clay mineral–water interface. *Environ. Sci. Technol.* **31**, 2005–2011.

Neuberger, C.S., Helz, G.R., 2005. Arsenic(III) carbonate complexes. *Appl. Geochem.* **20**, 1218–1225.

Nickson, R.T., McArthur, J.M., Ravenscroft, P., Burgess, W.G., Ahmed, K.M., 2000. Mechanism of arsenic release to groundwater, Bangladesh and West Bengal. *Appl. Geochem.* **15**, 403–413.

Nickson, R.T., McArthur, J.M., Shrestha, B., Kyaw-Myint, T.O., Lowry, D., 2005. Arsenic and other drinking water quality issues, Muzaffargarh District, Pakistan. *Appl. Geochem.* **20**, 55–68.

Nordstrom, D.K., Archer, D.G., 2003. Arsenic thermodynamic data and environmental geochemistry. In: a. S., A.H., Welch, K.G. (Eds.), *Arsenic in Ground Water: Geochemistry and Occurence*. Kluwer Academic Publishers, pp. 1–25.

Paul, K.W., Borda, M.J., Kubicki, J.D., Sparks, D.L., 2005. Effect of dehydration on sulfate coordination and speciation at the Fe-(hydr)oxide–water interface: a molecular orbital/density functional theory and Fourier transform infrared spectroscopic investigation. *Langmuir* **mm**, xy–xz.

Peak, D., Ford, R.G., Sparks, D.L., 1999. An in situ ATR-FTIR investigation of sulfate bonding mechanisms on goethite. *J. Colloid Interface Sci.* **218**, 289–299.

Persson, P., Axe, K., 2005. Adsorption of oxalate and malonate at the water-goethite interface: molecular surface speciation from IR spectroscopy. *Geochim. Cosmochim. Acta* **69**, 541–552.

Pierce, M.L., Moore, C.B., 1980. Adsorption of arsenite on amorphous iron hydroxide from dilute aqueous solution. *Environ. Sci. Technol.* **14**, 214–216.

Pierce, M.L., Moore, C.B., 1982. Adsorption of arsenite and arsenate on amorphous iron hydroxide. *Water Resources Res.* **16**, 1247–1253.

Raven, K.P., Jain, A., Loeppert, R.H., 1998. Arsenite and arsenate adsorption on ferrihydrite: kinetics, equilibrium, and adsorption envelopes. *Environ. Sci. Technol.* **32**, 344–349.

Rietra, R.P.J.J., Hiemstra, T., van Riemsdijk, W.H., 1999. Sulfate adsorption on goethite. *J. Colloid Interface Sci.* **218**, 511–521.

Rietra, R.P.J.J., Hiemstra, T., van Riemsdijk, W.H., 2001a. Comparison of selenate and sulfate adsorption on goethite. *J. Colloid Interface Sci.* **240**, 384–390.

Rietra, R.P.J.J., Hiemstra, T., van Riemsdijk, W.H., 2001b. Interaction between calcium and phosphate adsorption on goethite. *Environ. Sci. Technol.* **35**, 3369–3374.

Sahai, N., Sverjensky, D.A., 1997. Solvation and electrostatic model for specific electrolyte adsorption. *Geochim. Cosmochim. Acta* **61**, 2827–2848.

Smedley, P.L., Kinniburgh, D.G., 2002. A review of the source, behavior and distribution of arsenic in natural waters. *Appl. Geochem.* **17**, 517–568.

Stanforth, R., 1999. Comment on "Arsenite and arsenate adsorption on ferrihydrite: surface charge reduction and OH- release stoichiometry". *Environ. Sci. Technol.* **33**, 3695.

Stumm, W., 1992. *Chemistry of the Solid–Water Interface*. John Wiley and Sons., Inc.

Suarez, D.L., Goldberg, S., Su, C., 1998. Evaluation of oxyanion adsorption mechanisms on oxides using FTIR spectroscopy and electrophoretic mobility. In: Grundl, D.L.S.a.T.J. (Ed.), *Mineral–*

Water Interfacial Reactions: Kinetics and Mechanisms. ACS Symposium Series 715, pp. 136–178.

Sun, X., Doner, H.E., 1996. An investigation of arsenate and arsenite bonding structures on goethite by FTIR. *Soil Sci.* **161**, 865–872.

Sverjensky, D.A., 1993. Physical surface-complexation models for sorption at the mineral–water interface. *Nature* **364**.

Sverjensky, D.A., 2003. Standard states for the activities of mineral surface-sites and species. *Geochim. Cosmochim. Acta* **67**, 17–28.

Sverjensky, D.A., 2005. Prediction of surface charge on oxides in salt solutions: revisions for 1:1 (M^+L^-) electrolytes. *Geochim. Cosmochim. Acta* **69**, 225–257.

Sverjensky, D.A., 2006. Prediction of the speciation of alkaline earths adsorbed on mineral surfaces in salt solutions. *Geochim. Cosmochim. Acta* **70**, 2427–2453.

Sverjensky, D.A., Fukushi, K., 2006. Anion adsorption on oxide surfaces: inclusion of the water dipole in modeling the electrostatics of ligand exchange. *Environ. Sci. Technol.* **40**, 263–271.

Sverjensky, D.A., Sahai, N., 1996. Theoretical prediction of single-site surface protonation equilibrium constants for oxides and silicates in water. *Geochim. Cosmochim. Acta* **60**, 3773–3798.

Tossell, J.A., 1997. Theoetical studies on arsenic oxide and hydroxide species in minerals and in aqueous solution. *Geochim. Cosmochim. Acta* **61**, 1613–1623.

Villalobos, M., Leckie, J.O., 2001. Surface complexation modeling and FTIR study of carbonate adsorption to goethite. *J. Colloid Interface Sci.* **235**, 15–32.

Weerasooriya, R., Tobschall, H.J., Wijesekara, H.K.D.K., Arachchige, E.K.I.A.K.U.K., Pathirathne, K.A.S., 2003. On the mechanistic modeling of As(III) adsorption on gibbsite. *Chemosphere* **51**, 1001–1013.

Wijnja, H., Schulthess, C.P., 2000. Vibrational spectroscopy study of selenate and sulfate adsorption mechanisms on Fe and Al (Hydr)oxide surfaces. *J. Colloid Interface Sci.* **229**, 286–297.

Wilkie, J.A., Hering, J.G., 1996. Adsorption of arsenic onto hydrous ferric oxide: effects of adsorbate/adsorbent ratios and co-occurring solutes. *Colloid Surface* **107**, 97–110.

Williams, P.M., Price, A.H., Raab, A., Hossain, S.A., Feldmann, J., Meharg, A.A., 2005. Variation in arsenic speciation and concentration in paddy rice related to dietary exposure. *Environ. Sci. Technol.* **39**, 5531–5540.

Zhang, N., Blowers, P., Farrell, J., 2005. Evaluation of density functional theory methods for studying chemisorption of arsenite on ferrihydroxides. *Environ. Sci. Technol.* **39**, 4816–4822.

Zhang, P.C., Sparks, D.L., 1990. Kinetics and mechanisms of molybdate adsorption/desorption at the goethite/water interface using pressure-jump relaxation. *Soil Sci. Soc. Am. J.* **53**, 1028–1034.